AN ABSTRACT OF A THESIS

STRUCTURAL HEALTH MONITORING OF THE HERNANDO DESOTO BRIDGE

Justin Ryan Bravo Alexander

Master of Science in Civil Engineering

The Hernando DeSoto Bridge in Memphis, Tennessee, was implemented with a static-based structural health monitoring system. This was due to the seismic vulnerability and importance to travelers crossing the Mississippi River. Using specifically placed sensors throughout the structure, one objective was to examine the functionality and performance of the friction pendulum bearings implemented in a seismic retrofit. In addition, it was desired to track the bearing movements and member strains before, during and after a seismic event.

The implemented structural health monitoring system consists of strain gages, short-range displacement gages and long-range displacement sensors implemented on the west and east ends of the main arch section. Vibrating wire strain gages were placed on each member framing into the bearings to determine the force distributions. Vibrating wire short-range displacement gages were also installed at the east and west arch piers. Using the force distributions and thermal movements captured, the coefficient of friction in each bearing was calculated and compared to the design values. In addition, high-speed non-contact laser displacement sensors were installed at each bearing to more comprehensively track the bridge movements during a seismic event. All the sensor data is being visualized in a real-time monitoring display. The display also includes a basic alerting system with threshold criteria to aid in proactively detecting and addressing any anomalies that may occur on the structure.

The result of the bearing performance investigation for the west end (Pier A) indicated adequate performance. The coefficient of friction for the upstream and downstream bearings were 0.05 and 0.06, respectively. The design (installation) value was 0.06. In addition, the measured thermal movements of the west end bearings were within 10% of the theoretical movement. Bearing performance could not be determined at the east end (Pier C) as limited thermal movement was measured. Furthermore, relatively low member force build-up was measured. These responses were attributed to probable substructure movement. Tracking the substructure movement is proposed for system upgrades and future research on the Hernando DeSoto Bridge.

STRUCTURAL HEALTH MONITORING OF THE HERNANDO DESOTO BRIDGE

A Thesis

Presented to

the Faculty of the College of Graduate Studies

Tennessee Technological University

by

Justin Ryan Bravo Alexander

In Partial Fulfillment

Of the Requirements of the Degree

MASTER OF SCIENCE

Civil Engineering

May 2017

CERTIFICATE OF APPROVAL OF THESIS

STRUCTURAL HEALTH MONITORING OF THE HERNANDO DESOTO BRIDGE

by

Justin Ryan Bravo Alexander

Graduate Advisory Committee:

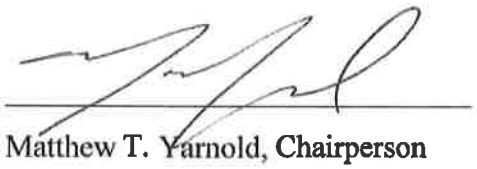

Matthew T. Yarnold, Chairperson — Date: 3/17/2017

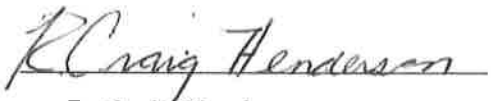

R. Craig Henderson — Date: 3/17/2017

Daniel R. VandenBerge — Date: 3/17/2017

Approved for the Faculty:

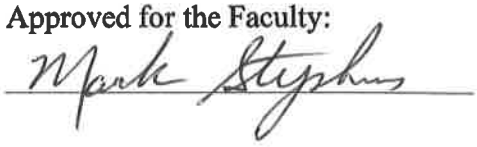

Mark Stephens

Dean

College of Graduate Studies

4/21/2017

Date

DEDICATION

This thesis is dedicated to my family for their never ending love, support and guidance they have continued to provide me in my pursuit of achieving my life goals. Without them, none of this would be possible.

ACKNOWLEDGEMENTS

I would like to sincerely thank my research advisor Dr. Matthew Yarnold for all his guidance and patience throughout my entire research project. You always made time to assist me whenever I was stuck with a challenge or needed some advice with my project, and I cannot thank you enough. Your enthusiasm and passion for bridges has provided me with a greater understanding and appreciation for bridges and for the structural health monitoring field.

I would like to thank the Tennessee Department of Transportation (TDOT) for funding this project and giving me the opportunity to perform this research. I would also like to thank Dr. Tim Huff with TDOT for providing me with pertinent structural information on the bridge and timely feedback on the instrumentation attachment designs for this project.

Thank you to Mr. Mark Davis with Tennessee Technological University for all your expertise and assistance in designing and fabricating the instrument attachment details for this project.

Thank you to Mr. Jim Bollwerk and his team from the Center for Earthquake Research and Information at the University of Memphis for all their assistance with our bridge reconnaissance, coordinating lane closures and usage of the Aspen A-62 snooper truck provided by the Tennessee Department of Transportation during our install, and providing on-site power to our system.

TABLE OF CONTENTS

Page

Page

LIST OF TABLES

Page

LIST OF FIGURES

Page

Page

CHAPTER 1

INTRODUCTION

Structural Health Monitoring (SHM) has grown in popularity as many countries around the world continue to grow their infrastructure. Early detection of deficiencies in a structure's performance through SHM has promoted safety for the public and allowed for more proactive approaches in locating and addressing issues with the structure. In a report card from the American Road and Transportation Builders Association (ARTBA), nearly 58,495 bridges were deemed structurally deficient or in need of repair in the United States in 2016, and 13 out of the 50 states had over 12% of their bridges determined to be structural deficient [1]. Some of these structures are inadvertently deficient due to the limitations of visual inspects or the length of time between inspections. SHM provides means to assess these structures on a regular basis in order to detect anomalies or deficiencies in the structure that may be undetectable with visual inspections. Due to their ability to send alerts for significant events or validate design efficiency with a structure's response to loads, SHM systems have become one alternative to manage old, new, and rehabilitated structures.

This research project included the design and implementation of a SHM system along the Hernando DeSoto Bridge. The Hernando DeSoto Bridge, built in 1973, is a two-span steel through arch bridge in Memphis, Tennessee that takes Interstate 40 over the Mississippi River and connects Memphis, Tennessee to West Memphis, Arkansas. In 2000, the Tennessee Department of Transportation (TDOT) partnered with the Arkansas

Figure 1.1 - Hernando DeSoto Bridge

State Highway and Transportation Department (AHTD) to retrofit the bridge for a seismic event due to it being a critical link for traffic crossing the Mississippi River and its proximity to the New Madrid Fault line. Both the Interstate 40 bridge (Hernando DeSoto) and the Interstate 55 bridge lie on the southeastern end of the New Madrid Seismic Zone, which is the most active seismic zone in the Central United States, and are the only two bridges that cross the Mississippi River within an 85-mile radius of their locations. The Hernando DeSoto Bridge main section can be seen in Figure 1.1.

Initially, a retrofit for the Interstate 55 Bridge was considered, but it was ultimately determined that the bridge could not be retrofitted. Because of this, keeping the Hernando DeSoto Bridge standing became a high priority for Tennessee and Arkansas. The seismic retrofit protects the bridge from earthquakes with a moment magnitude of up to 7.7 [2]. Because of the retrofit and the structure's importance to travelers crossing the Mississippi River, in 2004 TDOT funded a vibration-based seismic monitoring program installed and maintained by the University of Memphis [3]. The vibration system includes acceleration

measurements at 36 different locations along the bridge. Then in 2015, TDOT funded the research presented herein to design and implement a static-based SHM system on the Hernando DeSoto Bridge that can identify the current performance of the bearings as well as track the bridge behavior before, during, and after a seismic event. The overall goal of the SHM system is to monitor the structure to provide TDOT with information for proactively preserving the structure long-term.

The primary specific objectives of this research project were as follows:

1. Design of a static-based SHM system: This included the determination of the measurement forms and locations along with the purchase of the equipment and pre-assembly in the laboratory.
2. Installation of the SHM system: Prior to install, programming of the data acquisition system was performed. Then, installation strategies and attachment details were developed. Finally, the system was physically installed along the bridge and quality control checks were performed.
3. Processing and interpretation of the data: This task established the current performance of the bearings along with typical force distributions within instrumented members. A framework was developed with threshold criteria for the future automated SHM system (automation not part of this thesis project).
4. Real-time monitoring display: A real-time visual display of the data was developed. This display shows time history plots and correlation diagrams of the data to illustrate the recent and current performance. Alarms are included in the display to

indicate sensor malfunction or data anomalies that require further evaluation. In addition, protocols were established for a structural performance evaluation after a seismic event.

CHAPTER 2

LITERATURE REVIEW

2.1 Introduction

Structural health monitoring is an active field of research which has an array of different system types and techniques for monitoring a structure. Monitoring systems for bridge structures are typically vibration-based, static-based and/or temperature-based systems and have been implemented on new, old, and rehabilitated structures [4]. Vibration based systems involve capturing acceleration measurements throughout the structure, while static-based systems or temperature-based systems typically capture the strains and displacements produced by various inputs. Some systems are implemented as a combination of the two in order to reap the benefits of both types of systems and monitor the structure more thoroughly. Multi-modal systems are very beneficial in acquiring valuable data on the structure, however they tend to be expensive to install and maintain. These types of systems were examined and reviewed in this study.

2.2 Vibration-Based Systems

Vibration-based systems typically include acceleration measurements at many discrete locations along the structure [5]. These types of SHM systems have been implemented on large structures with particular vulnerabilities such as earthquakes and high wind speeds [3,5]. Vibration based systems have been determined to be an effective way of identifying structural deficiencies but tend to be strayed away from in monitoring large structures with substantial amounts of environmental variability and operational use due to the effects that temperature and operational use have on the structure's modal frequency [6,7]. This change in modal frequency makes it difficult to determine the baseline frequency of the structure, and therefore increases the difficulty of determining any damage to the structure and where the damage is located. For this reason, vibration-based systems have limited capabilities on large structures.

2.3 Static-Based Systems

Static-based systems have shown to be an effective strategy for SHM systems. Typically, static-based systems utilize strain, displacement, and/or tilt angle measurements using resistance-based sensors [8], vibrating wire technology [9] or fiber optic systems [10]. Fiber optic systems have grown in popularity because of their high precision level and immunity to electrical and magnetic noise [11], fiber Bragg grating sensors [12], but these systems tend to be expensive and harder to justify in many cases. Some long-term static-based systems focus on tracking the thermal signature of the structure. These temperature-driven monitoring systems use thermal data to assess critical moving

mechanisms on structures such as expansion joints, bearings, etc. [13]. Because bearing health has become a vital variable to a bridge structure's long-term durability [14], research by Yarnold and Dubbs was done with Periodic Temperature-Based Systems in SHM on a steel-tied arch bridge to aid visual inspections in bearing health assessment [15]. The objective of the study was to assess the bridge structure's bearing health or bearing performance without the use of a finite element model using specifically placed sensors in order to obtain the strains in members framing into the bearings and the movement experienced in the bearings due to temperature changes. With visual inspections being the primary assessment tool for bearing health, the authors indicated that bearing issues go unseen until significant damage on the bridge structure has already occurred [15]. Through analyzing the data, they were able to assess the functionality of the bearings based on the structure's temperature movements and compare bearing design characteristics with actual measurements.

2.4 Multi-Modal Systems

Multi-modal SHM systems have recently been researched and implemented on various bridge structures. Cachot et al. (2015) produced a 10 year-long study on the Millau Viaduct in France [16]. The Millau Viaduct is a multi-span cable-stayed bridge in southern France that consists of 8 spans and stretches over 8,000 feet. To optimize the life of the structure, the monitoring system was composed of a static-based system, a dynamic system and a temperature based system that was implemented onto the structure during

construction and once the structure was in operational use. Many SHM systems on large structures have become multi-modal as many technologies advance due to research and as various system types become more affordable. The Tsing Ma Bridge, located in Hong Kong, China, is the longest suspension bridge in the world and has had a conventional Wind and SHM system implemented on it since May 1997 [17]. The conventional system consisted of accelerometers, strain gages, displacement transducers, level sensors, anemometers, temperature sensors and weigh-in-motion sensors. Because fiber optic systems have become more economically feasible, in May 2003 a fiber optic system consisting of 40 fiber Bragg grating (FBG) sensors were implemented to monitor the structure and validated the functionality of the existing SHM system [17]. In conclusion, combined systems have shown to be beneficial in preserving the health of large bridge structures with various types of environmental vulnerabilities.

CHAPTER 3

HERNANDO DESOTO BRIDGE BACKGROUND

The Hernando DeSoto Bridge is a 19,535 foot (3.7 mile) long bridge that runs East and West over the Mississippi River connecting Memphis, Tennessee to West Memphis, Arkansas. The section of the bridge that is focused on in this research is the main section which is a 1,800 foot, two-span steel through arch bridge. The steel through arch bridge or main section is located in the state of Tennessee and consists of two 900 foot spans with three piers: Pier A, Pier B, and Pier C. An overview of the main section of the bridge can be seen in Figure 3.1.

The bridge is 93 feet wide with six lanes consisting of three westbound and three eastbound lanes. A typical cross-section of the bridge can be seen in Figure 3.2.

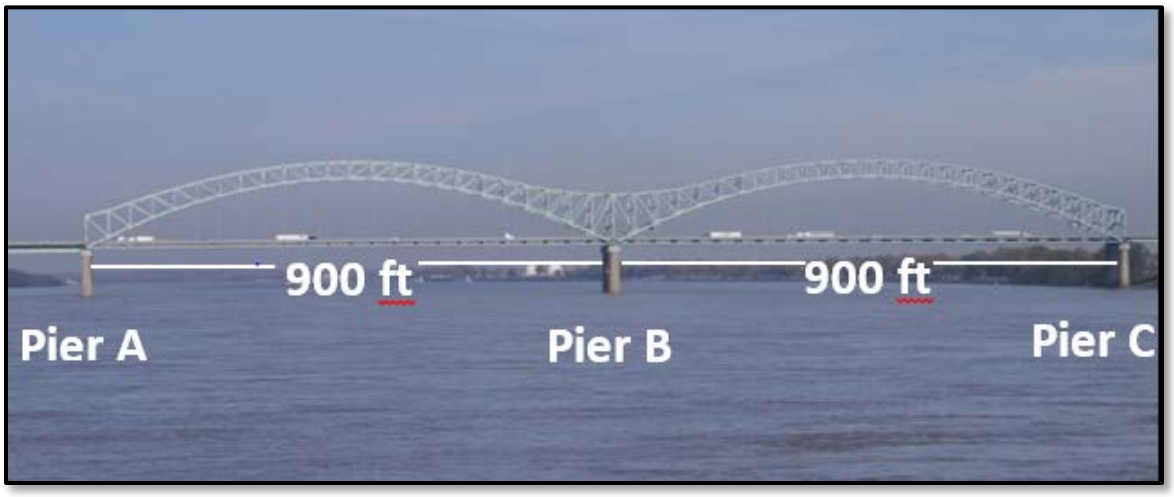

Figure 3.1 - Main Section of Hernando DeSoto Bridge

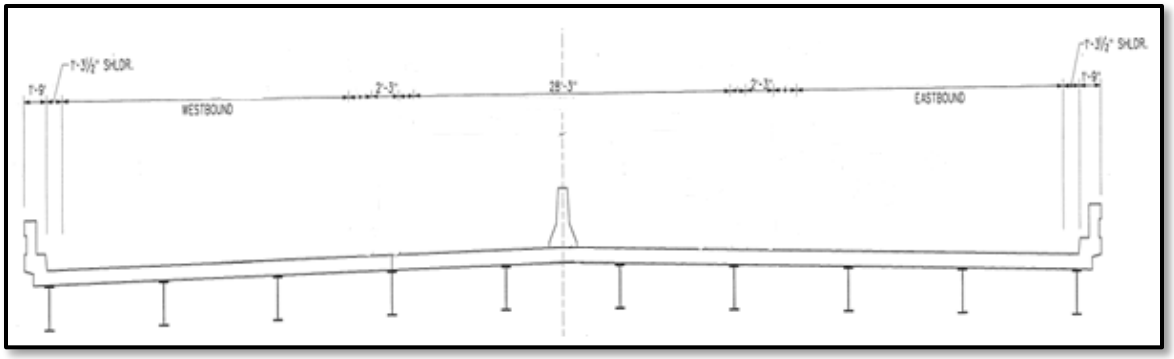

Figure 3.2 - Hernando DeSoto Bridge Cross-Section

The overall focus of the project was instrumenting and monitoring the bearing movements and the force distribution in the arch members at Pier A and Pier C. A cross-section of the bridge at Pier A and Pier C showing the instrumented bearings can be seen in Figure 3.3 and Figure 3.4.

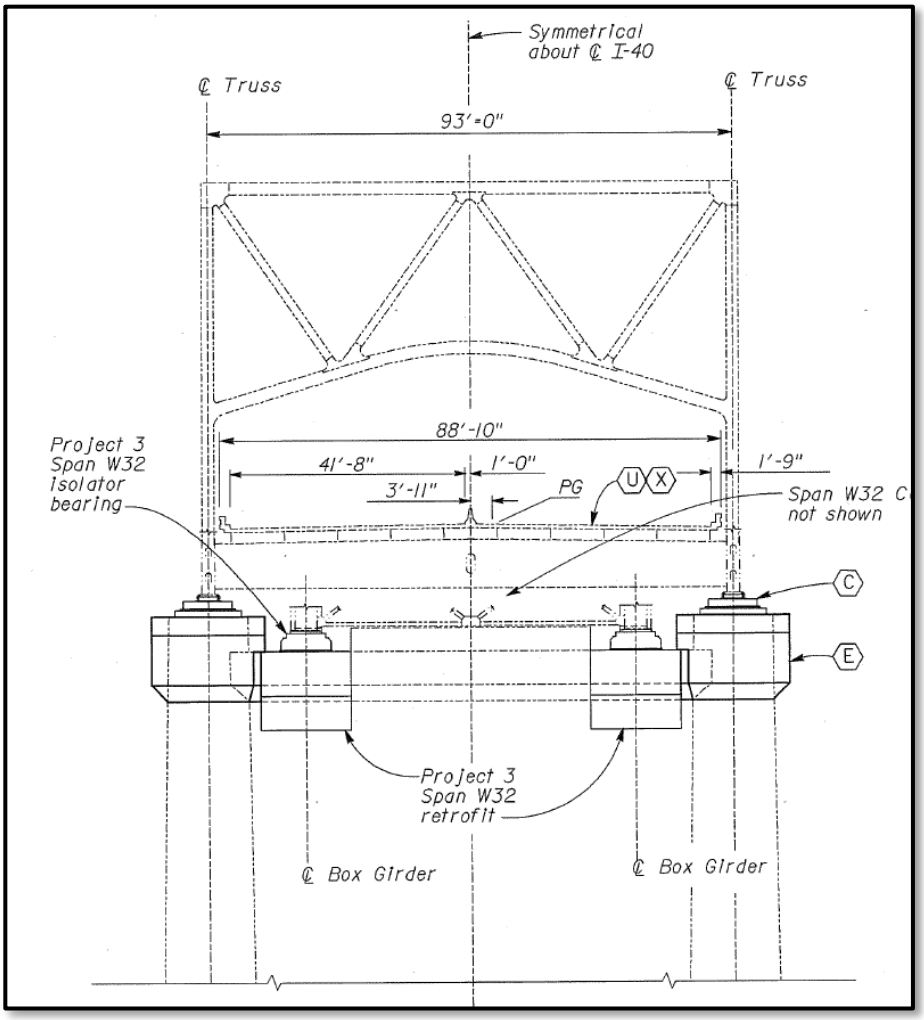

Figure 3.3 - Pier A Cross-Section

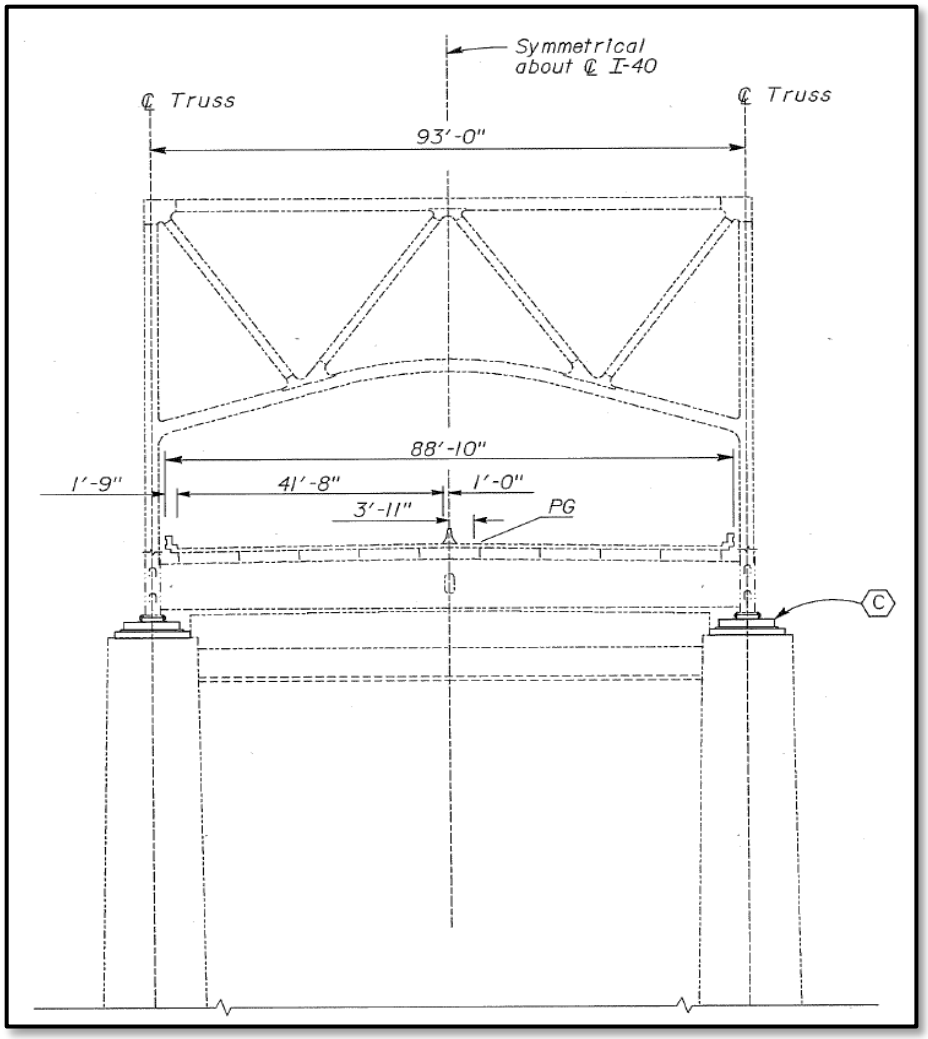

Figure 3.4 - Pier C Cross-Section

The main instrumented arch members at Pier A and Pier C are box-shaped, built-up members that are bolted into gusset plates as they frame into the bearings. The three members from the main arch were instrumented in order to develop the force distribution framing into the bearings. These members are labeled as the vertical, diagonal and bottom chords. The loads produced by the superstructure are transferred through the main arch members and then into the substructure through the bearings. By instrumenting and studying the force distribution in these members, bearing design characteristics such as the

Figure 3.5 – Arch Member Framing into the Bearing

coefficient of friction can be determined and validated. An example of the members framing into the bearings can be seen in Figure 3.5.

During the seismic retrofit conducted by TDOT and AHTD in 2000, a base-isolation system was implemented using base-isolation friction pendulum bearings to increase the structure's seismic capacity due to its proximity to the New Madrid Seismic Zone. Out of the eight friction pendulum bearings implemented onto the main section, four were implemented at Pier A, two at Pier B, and two at Pier C. These friction pendulum bearings implemented on the main section of the bridge lengthen the natural period of the structure to help isolate the superstructure during any ground acceleration and dampen the lateral forces created by an earthquake. The bearing at rest and at maximum displacement can be seen in Figure 3.6 and Figure 3.7.

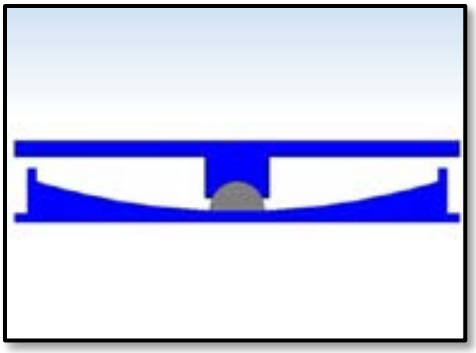

Figure 3.6 - Friction Pendulum Bearing at Center Position

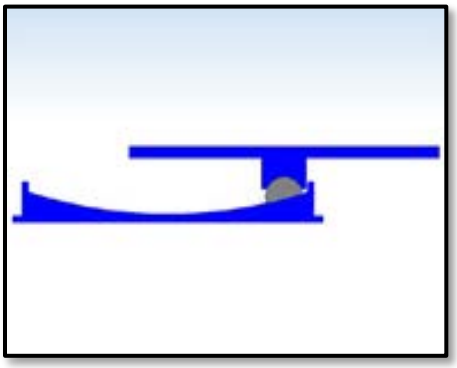

Figure 3.7 - Friction Pendulum Bearing at Maximum Displacement

Using a pendulum concept, the bearings are designed with a half-circle slider, a concave bottom surface, and cap on top of the slider to support the superstructure. During an earthquake, the bearings isolate the superstructure and allow the superstructure, which is connected to the top of the slider, to slide back and forth in a pendulum like motion on the concave bottom surface. Because of the semi-circle shaped slider, gravity keeps the weight of the supported superstructure centered as it moves on the concave surface, allowing the superstructure to stay level once in motion. Over time, the lateral forces induced on the structure by an earthquake will dampen due to the coefficient of friction designed within the concave surface of the bearing until the structure ceases to move. Not only does the concave surface allow the structure to move in a pendulum like motion but centers the

structure post movement as gravity brings it to the bottom of the bowl-shaped surface. Therefore, due to the significant role the bearings have on the structure's seismic capacity, significant time and research was conducted to evaluate whether the bearings were performing as designed.

CHAPTER 4

METHODOLOGY

The overall objective of this study was to provide TDOT with a static-based SHM system that has the ability to identify the current performance of the bearings as well as track the bridge behavior before, during, and after a seismic event. In order to accomplish this objective, the study was to be broken into the instrumentation design (Chapter 5), SHM system installation (Chapter 6), data processing and interpretation (Chapter 7), and the development of a long-term monitoring system with a real-time display and post-event data acquisition (Chapter 8).

The first task was to design an instrumentation plan for the static-based monitoring system that would identify the bearing performance. This was achieved through measurement of the bridge movements due to temperature change along with the thermal forces within the arch members framing into the bearings. In addition, it was desired for the system to have the ability to capture the bridge movements before, during, and after a seismic event. As a result, the first set of instrumentation chosen was vibrating wire (VW) strain gages and VW displacement gages to track the bridge movements and forces due to temperature change. Because of the large and rapidly changing displacements the bridge is able to experience through a seismic event with the implemented friction pendulum bearings, VW gages were not used in this aspect of the instrumentation design. Instead

non-contact laser displacement sensors were implemented to monitor the bearing movements during a seismic event. These sensors are capable of measuring large ranges of movement at faster rates. In addition, they provide redundancy in the system's ability to track the bearing temperature movements.

The next step was to develop a program for the system that would obtain measurements from the implemented gages, convert the acquired data values into customary units, and wirelessly send the data to Tennessee Technological University to be analyzed. In order to do so, each strain gage, displacement gage and non-contact displacement gage was connected to the system's data logger where the gages were programmed and evaluated for errors. The troubleshooting of these gages were performed until each gage reading equated to what was desired. The system was then assembled in an organized manner into two boxes, Box A and Box C, where they would later be implemented onto the structure to acquire the measured data and wirelessly transmit it to be studied. Once the system was assembled, data quality checks were performed to ensure the system would operate optimally post-installation.

The third step was to implement the designed and assembled SHM system onto the Hernando DeSoto Bridge. A lane closure road crew and the use of the Aspen A-62 snooper truck were coordinated with TDOT in order to have accessibility to desired locations on the bridge. During the span of five days, four days consisted of instrumentation attachments, soldering and cabling from gage to box location, box attachments and system wire assembly. The fifth day was used to perform quality control checks on the

instrumentation attachments, the box assemblies and the acquired data from the system to try to eliminate any sensor malfunctions.

Once the instruments were programmed and installed on the bridge, data was processed and interpreted to determine the behavior of the structure. Providing TDOT information on the performance of the friction pendulum bearings installed during the retrofit of the structure in 2000 is one of the main objectives of this study. With this data, design values such as the coefficient of friction in the bearings were compared with the actual measured values to determine if the functionality of bearings matched the design. In addition, the thermal movement was compared to the theoretical values.

This SHM system design also has a seismic monitoring component that has the ability to track and monitor the bearing behavior before, during, and after a seismic event through the laser tracking devices. A real-time monitoring display was developed with thresholds and a basic alerting system identifying what thresholds were exceeded. To supplement this, a post-event data acquisition plan was developed for detailed analysis.

CHAPTER 5

INSTRUMENTATION DESIGN

5.1 Introduction

To begin designing the system, research was done on the instrumentation, such as the strain and displacement gages, data loggers, and radios, to verify whether these instruments were suitable for this specific project and application. Several different options were considered in designing the instrumentation, and the best combination was selected for the monitoring system. The overall instrumentation plan and how these instruments of the SHM system were programmed and assembled are discussed in the next section of this chapter.

5.2 Instrumentation Plan

An instrumentation plan was designed to effectively identify the bridge temperature movements and movements due to an earthquake. In order to accomplish this objective, strain gages, short-range displacement gages, and non-contact displacement gages were selected for locations on Pier A and Pier C to optimize the quality of data obtained in this

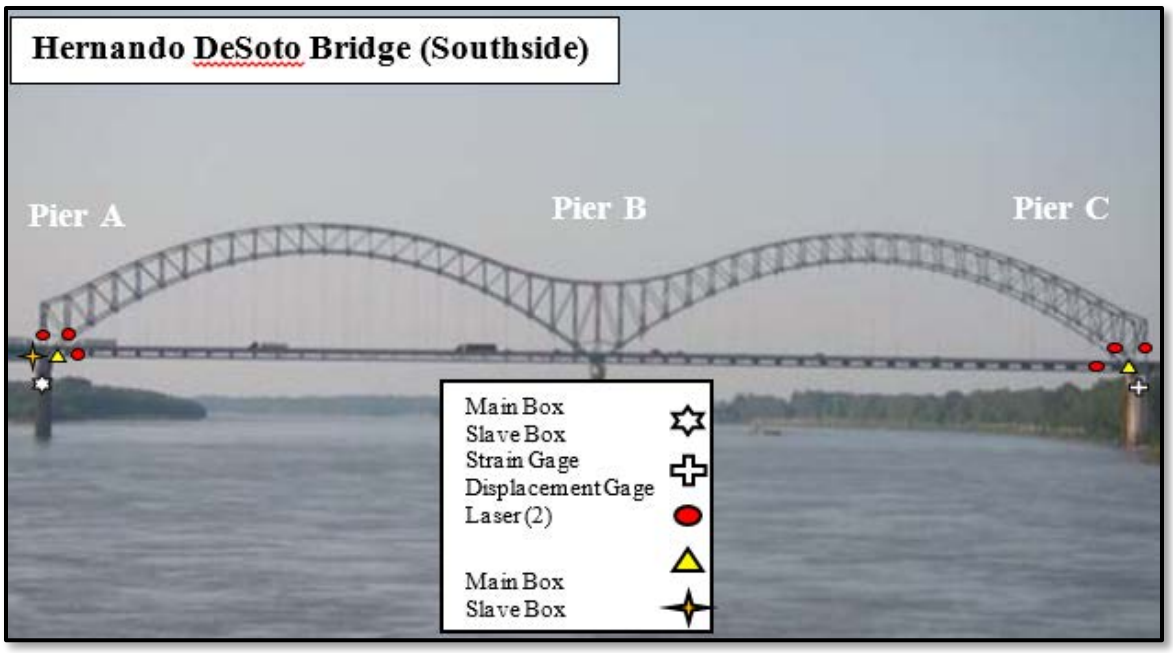

Figure 5.1 - Instrumentation Overview (Southside)

research. An overview of the instrumentation design on the structure is shown in Figure 5.1. The instrumentation design for this static-based SHM system consisted of 24 strain gages, 6 displacement gages, 30 thermistors and 4 lasers that were implemented on Pier A and Pier C of the bridge. The number of each type of gage placed on Pier A and Pier C and an overview of the instrumentation at Pier A and Pier C can be seen in Table 5.1, Figure 5.2 and Figure 5.3. Note the sensors in Figure 5.2 and Figure 5.3 are on the South side and are identical on the North side of each pier. All the VW sensors and lasers on Pier A are cable connected to a data logger located on Pier A.

Table 5.1 - Instrumentation

Pier	Strain Gage	Displacement Gage	Lasers	Thermistor
A	12	4	4	16
C	12	2	0	14

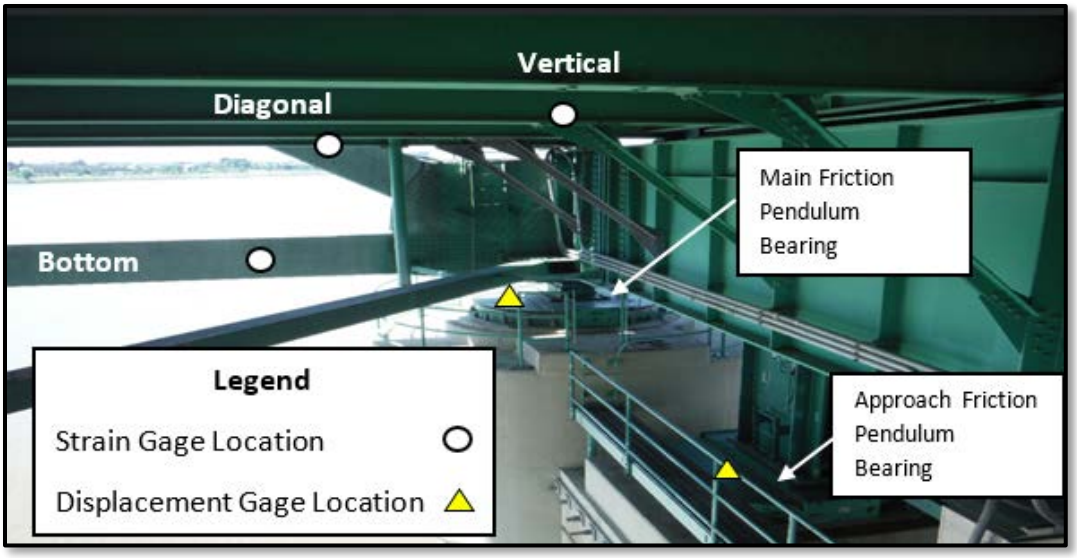

Figure 5.2 - Pier A Instrumentation (Southside)

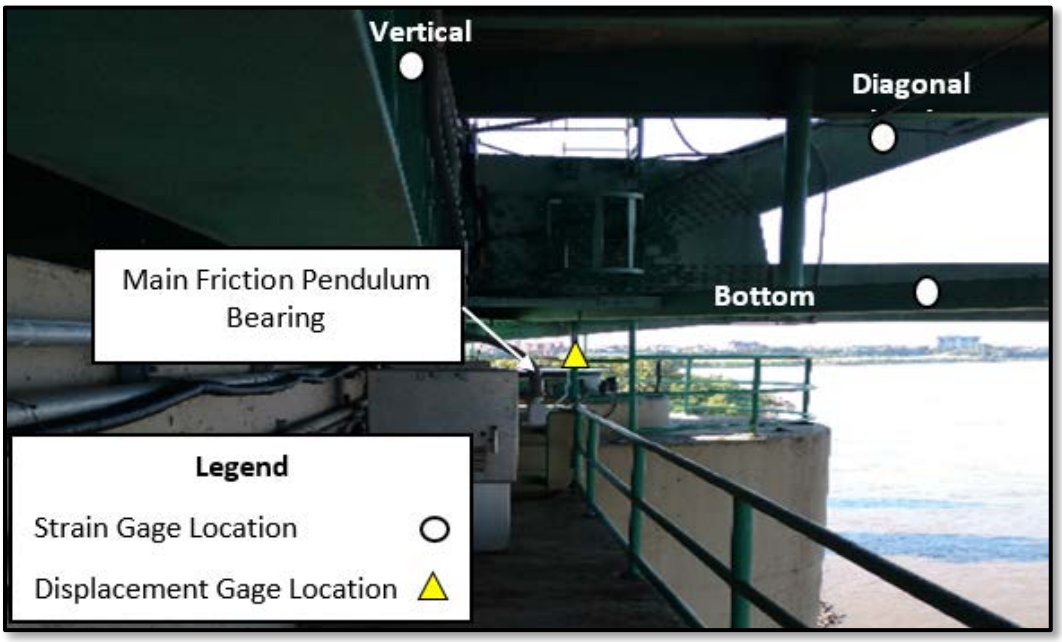

Figure 5.3 - Pier C Instrumentation (Southside)

As for the sensors on Pier C, they are cable connected to a setup on Pier C that wirelessly sends data to the data logger located on Pier A. The data logger on Pier A is connected to a cell modem which provides remote accessibility anywhere with an internet connection. The data logger is programmed to sample the readings of the strain and displacement gages

once every five minutes. Sampling every five minutes produces sufficient data to analyze the temperature movements of the structure. The focus of these measurements is to assess the functionality of the bearings and determine the force distribution of the arch members framing into these bearings.

Along each cross-section of members framing into the friction pendulum bearings on Pier A and Pier C, six Geokon Model 4000 VW strain gages were attached to measure the strain experienced in the members. The strain gages can be seen in Figure 5.4. Each strain gage has a thermistor to take temperature measurements along with the strain measurements. Two strain gages were attached to the roadway side of each member cross-section, eight inches from the top and bottom of the member. This was done in order to not only have the ability to monitor the axial behavior of the members but to monitor its in-plane bending behavior, as well as provide redundancy in the measurements. The VW strain gages were attached roughly five feet from the gusset plates to reduce the gusset plate influence on the strain data. A view of a typical strain gage location from the catwalk of the structure is shown in Figure 5.5.

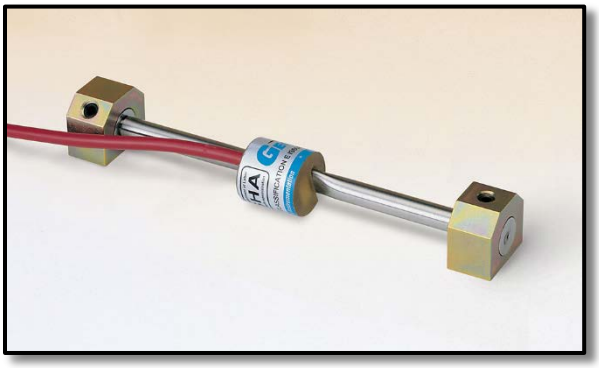

Figure 5.4 - Geokon Model 4000 Strain Gage

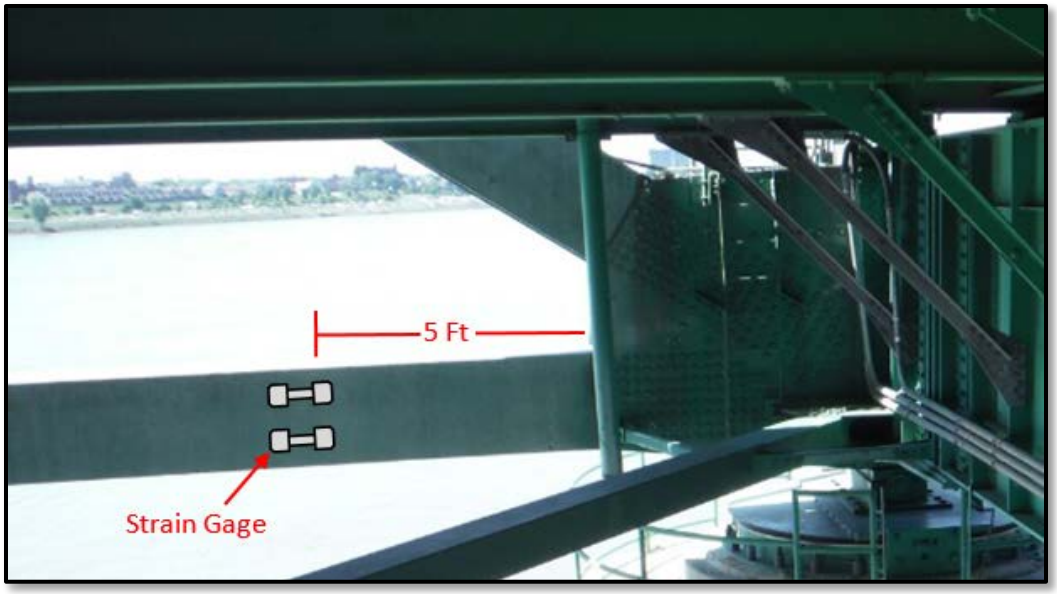

Figure 5.5 - Typical Strain Gage Placement on Member

VW displacement gages were utilized to act as the short-range displacement gages that track the temperature movements experienced in the friction pendulum bearings. The short-range displacement gages used in this project are the Geokon Model 4420 customized with a specific range to withstand the projected temperature movements of the superstructure. Like the strain gages, thermistors are also included with each displacement gage to track the temperature as the bridge expands and contracts. The VW displacement gage is shown in Figure 5.6.

Figure 5.6 - Geokon Model 4420 Displacement Gage

To size the displacement gages for the movement range needed for this application, the equation for linear thermal expansion was used. Assuming Pier B is fixed, the theoretical longitudinal displacement (δ) at Pier A and Pier C for the 900 foot span lengths were calculated using the expression in Eq. 1. Assuming a coefficient of thermal expansion for steel as roughly 6.5e-6 in/in°F and a conservative uniform temperature change of 120°F, the expression yields a movement range of 8.4 inches (213 mm). As a result, the displacement gage range selected for this project was conservatively 250 mm (9.8 inches).

$$\delta = \alpha(\Delta T)L \qquad \textbf{Eq. 1}$$

where, α = coefficient of thermal expansion of steel
ΔT = uniform change in temperature
L = span length

Since the structure is in a high seismic zone, Acuity AR1000 Lasers were implemented into the design as the non-contact displacement gages to track the larger potential movements of the structure due to an earthquake. Knowing the bearings ability to displace longitudinally a maximum of 32 inches and laterally a maximum of 27.25 inches, selecting the right long-range displacement gages for this application became a challenge. Long-range VW gages were considered but were deemed impractical due to their delicate range capabilities and attachment difficulties. To meet this challenge, two lasers were placed at each bearing on Pier A, one parallel and one perpendicular to the bridge to track the longitudinal and lateral movements of the superstructure. In order to capture the relative movement of the superstructure to the substructure/pier during an earthquake, the lasers were programmed to sample at a frequency of 10 Hertz. A higher

sampling rate was desired, however, limitations with the data logger required this maximum sampling rate. Due to the location of the bearings relative to the entire structure, measuring the bearing's absolute movement became a task that seemed impractical to solve. Sampling at this rate will produce sufficient data to analyze and assess the movements of bearings before, after, and during the event.

5.3 System Programming and Assembly

After the instrumentation plan was finalized, the instruments were ordered and shipped to the laboratory for programming and assembly. First, the data logger, a Campbell Scientific CR1000, was programmed using a Campbell Scientific software called LoggerNet. LoggerNet was used to communicate with the CR1000 and send new and updated programs as the system was being assembled. A copy of the final program used for the monitoring system can be seen in Appendix A. These programs were developed within LoggerNet using a CR Basic programming language. The CR1000 data logger is shown in Figure 5.7.

Figure 5.7 - Campbell Scientific CR1000 Datalogger

The program was constructed with intentions to have the CR1000 acquire measurements from the gages instrumented on Pier A that were directly hardwired into the datalogger and acquire measurements wirelessly by radio from a set up wired to the gages instrumented on Pier C. To have the gages on Pier A hardwired into the data logger, a Campbell Scientific vibrating wire analyzer (AVW200) and a Campbell Scientific Multiplexer were wired into the CR1000 to increase the number of gages that could be directly connected to the CR1000. This Multiplexer permitted the instrumentation design to have the designed 20 gages on Pier A directly hardwired into the system. In addition, a back-up battery, a cell modem and a radio were installed for remote access to the system and for communication between the setup at Pier A and Pier C. The Box A configuration can be seen in Figure 5.8.

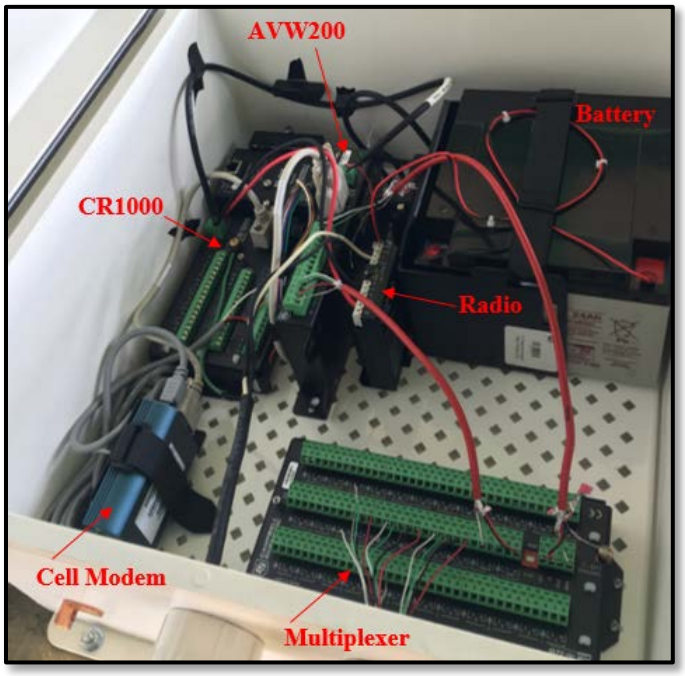

Figure 5.8 - Box A Configuration

For the setup on Pier C, Box C consisted of a Campbell Scientific vibrating wire analyzer which included a built in radio (AVW206), a Multiplexer and a back-up battery for any instances that direct power was not available. The AVW206 was programmed to obtain the gage measurements at Pier C, and through its built in radio, send the gage measurements to Box A where it was received and stored by the CR1000. The CR1000 would then store the collected data, and when accessed, allow the data to be downloaded remotely. The configuration of Box C can be seen in Figure 5.9. In order to program the system to perform these tasks, significant time was devoted to the development of the program and assembly of this complex system. Data quality checks and assembly checks were conducted to help eradicate any possible issues that inhibit a successful installation process and ensure its performance is as designed.

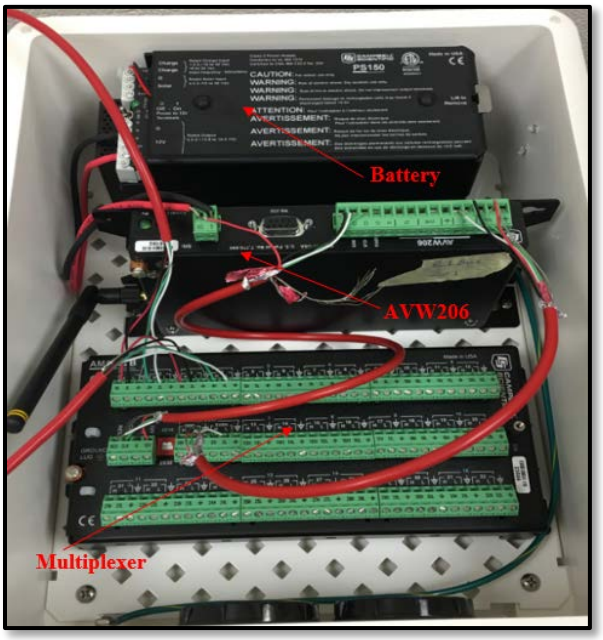

Figure 5.9 - Box C Configuration

CHAPTER 6

SHM SYSTEM INSTALLATION

6.1 Introduction

The second objective of this project was to install the instrumentation onto the Hernando DeSoto Bridge. This included the development of an attachment method for each element of the monitoring system, fabrication of the attachments for each designed method, coordination with TDOT for lane closures and the use of their Aspen A-62 snooper truck, and the execution of quality control checks after installation. The installation of the instrumentation consisted of four days with a fifth day designated for quality controls checks on the data and the attachments. An overview of the installation of the system is discussed in the next section followed by detailed information on the attachment methods.

6.2 Installation Overview

Over the four days of installation, TDOT provided lane closures with a road crew on east and west bound traffic lanes for safety during the installation of the system and to allow the use of their Aspen A-62 snooper truck. The use of the snooper truck was vital in

Figure 6.1 - Aspen A-62 Snooper Truck and Road Crew

executing the instrumentation design because it allowed access to all gage locations on the bridge. Figure 6.1 illustrates the lane closure during the use of the Aspen A-62 snooper truck.

Days one and two were designated for the installation of the system on Pier A. Using the Aspen A-62 snooper truck, strain gages were attached to the arch members framing into the upstream and downstream friction pendulum bearings. The use of the snooper truck during the attachment of the strain gages is shown in Figure 6.2.

Figure 6.2 - Snooper Truck Use during Strain Gage Attachment

Displacement gages and lasers were then attached at their designed locations. Once all the gages were attached, the cabling was performed to run the wires from the gages to Box A's location. Since extra cabling was needed for some of the gages to reach the Box A location, time was devoted to soldering the extra cable lengths. Once all the gages were attached and the extra cable was soldered, Box A was mounted onto the pier cap using one-fourth inch wedge anchors. Because the system was designed for the CR1000 in Box A to receive information wirelessly from Box C, a clear line-of-sight was needed between Box A and Box C to have information transmitted and received properly. To accommodate this, Box A was mounted on the top surface of the pier cap. The box location and line-of-sight to Pier C can be seen in Figure 6.3.

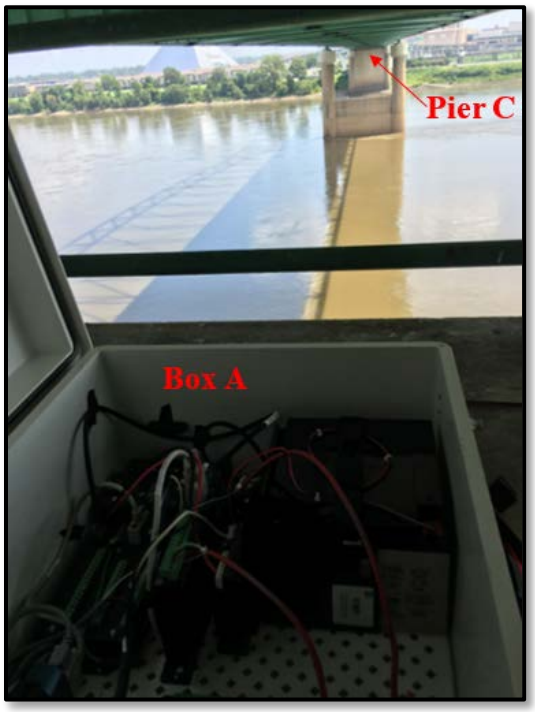

Figure 6.3 - Box A Line-Of-Sight to Pier C

Figure 6.4 - Box A Post Installation

The strain and displacement gages were then wired into specific channels on the Multiplexer while the lasers were wired directly into the CR1000 within Box A. This was done due to the difference in sampling rates. Because each gage had to be wired into the correct channel for the system to work as designed, considerable time was dedicated to ensure the wiring was done correctly. Figure 6.4 depicts Box A post installation.

After the installation of the instrumentation on Pier A, days three and four were devoted to the installation of the system on Pier C. Similar to Pier A, the strain gages were attached on the arch members using the Aspen A-62 snooper truck provided by TDOT, and displacement gages were attached to the upstream and downstream friction pendulum bearings. No soldering was needed as ample cabling was available to reach the location of Box C. Once the gages were attached, Box C was mounted, and the gages were wired to their designated channels on the Multiplexer. The cabling was then put in the flexible

Figure 6.5 - Box C Post Installation

conduit for environmental protection and aesthetics. Figure 6.5 depicts Box C during post installation.

The fifth day of the installation was devoted to performing quality control checks on the system. Gage attachments and wiring were scrutinized in order to ensure the gage wires were in the correct channels and that gages were attached correctly. Superglue was applied on nuts and bolts on the attachments to prevent any back-off from occurring due to long-term vibration experienced on the bridge. Specifics of the superglue application is discussed in the next section.

6.3 Attachment Method Details

In designing the attachment methods for each gage within the SHM system, each attachment method was detailed and presented to TDOT for approval. Once approved, materials were gathered for the attachments and fabricated to the specifications presented to TDOT. The most non-destructive methods were selected for this project.

To begin the attachment method of the strain gages, the locations of the gage mounting blocks were marked on the arch member, and the paint was grinded off to ensure a good contact between the gage and the member. The gage and the attached mounting blocks can be seen in Figure 6.6.

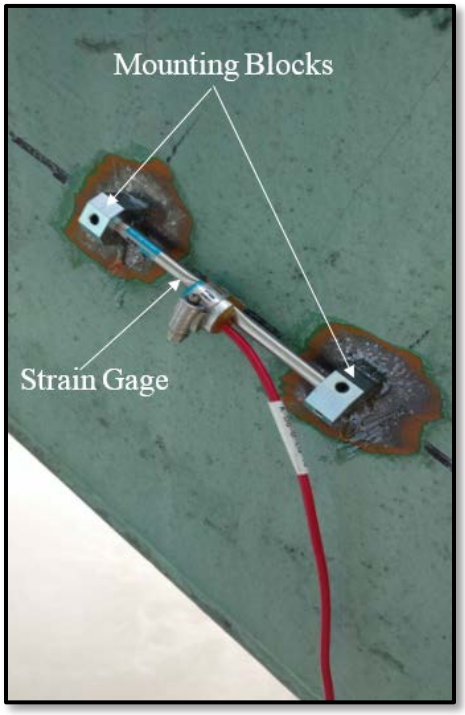

Figure 6.6 - Strain Gage and Mounting Blocks

Figure 6.7 - Steel Gage Covers

Next, fast-setting superglue was applied to the mounting blocks to attach the gage to the member. Once the superglue dried, a high strength epoxy was applied around the back and sides of the mounting blocks. This attachment method is relatively easy and a good non-destructive alternative to attaching these gages. After allowing for a five-minute setting time for the epoxy, two coats of UV-resistant spray paint were applied onto the gage, and a steel cover was placed over the attachment to protect the gages and attachment. The steel covers can be seen in Figure 6.7 above. The steel covers were attached similarly to the gages in that superglue and epoxy was used, but the paint on the bridge was not grinded off. Once the gages and covers were attached, the cables for these gages were placed in flexible conduit (wire loom) throughout the bridge for cable protection and aesthetics. A portion of the black flexible conduit that was used in this project is shown in Figure 6.7.

The attachment process of the short-range VW displacement gages was a difficult process to develop in that one end of the gage had to be attached to the substructure and the other end attached to the superstructure in order to capture the relative movement experienced in the bearings. To accomplish this task, four 22-inch tall steel brackets were

fabricated to be anchored onto the pier cap (substructure) and bolted to one end of the gage. The other end of the gage was bolted to a steel angle attached to the top of the bearing (superstructure). To attach the angle to the bearing, the angle was first centered on the bearing. Once centered, the location of the angle was marked and grinded to clear off any paint or debris. Superglue and fast-setting epoxy was then applied to the angle to secure the angle to the bearing. While allowing for the superglue and epoxy on the angle to cure, the fabricated bracket was centered to the angle and marked. Holes were drilled into the pier cap in order to anchor the brackets securely. One-fourth inch wedge anchors were hammered into the drilled holes, and the bracket was bolted onto the pier cap. The VW displacement gage was then bolted at the ends to both the angle, which was attached to the superstructure, and the bracket which was attached to the substructure. The attachment of the gage and brackets can be seen in Figure 6.8.

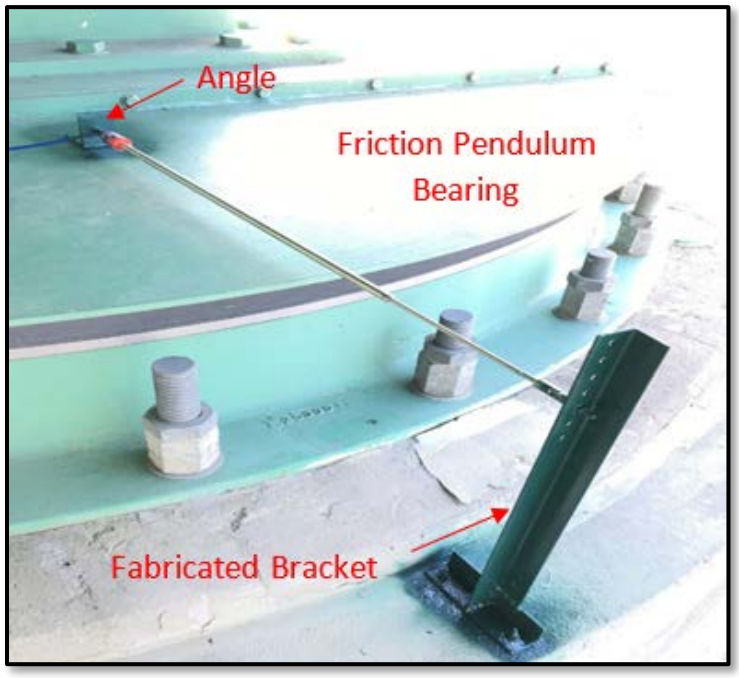

Figure 6.8 - Displacement Gage Attachment

Some preventive care was done to protect the attachment from corrosion and vibration. Three coats of UV-protective spray paint were applied to the connections and bolts in order to protect the connection from UV rays and corrosion. To help prevent any backing off of the nuts on bolts due to the vibration experienced on the bridge, superglue was applied to the contact between the nuts and bolts holding the gage to the attachments and holding the bracket to the pier cap.

The attachment of the lasers (or non-contact displacement gages) was difficult because (1) the lasers had to be secured onto a stationary structure for accuracy of the data and (2) a large flat surface on the bearings had to be found to have the lasers to target. With an uneven surface, the laser readings would be sporadic with data interpretation being difficult due to the inconsistency of the readings. It would be difficult to determine if the spikes in the readings were due to actual movements in the bearings or changes in depth of the surfaces the lasers were targeting. To ensure the lasers would stay stationary, aluminum

Figure 6.9 - Acuity AR1000 Laser and Attachment

railing brackets were fabricated with four one-fourth inch drilled holes for the lasers to be bolted down. The aluminum brackets were attached to the pier cap railings using pipe clamps that wrapped through the attachment and around the railings. The laser and the attachment is shown in Figure 6.9. Once the attachments were secured, the lasers were pointed at the desired flat surface on a selected side of the bearings and bolted onto the aluminum brackets. Superglue was also applied to the pipe clamps and bolts to prevent the nuts from backing off due to vibration experienced on the bridge. Figure 6.10 illustrates the perpendicular and parallel orientations of the Acuity AR1000 Lasers on the pier cap to effectively capture any bearing movements from an earthquake.

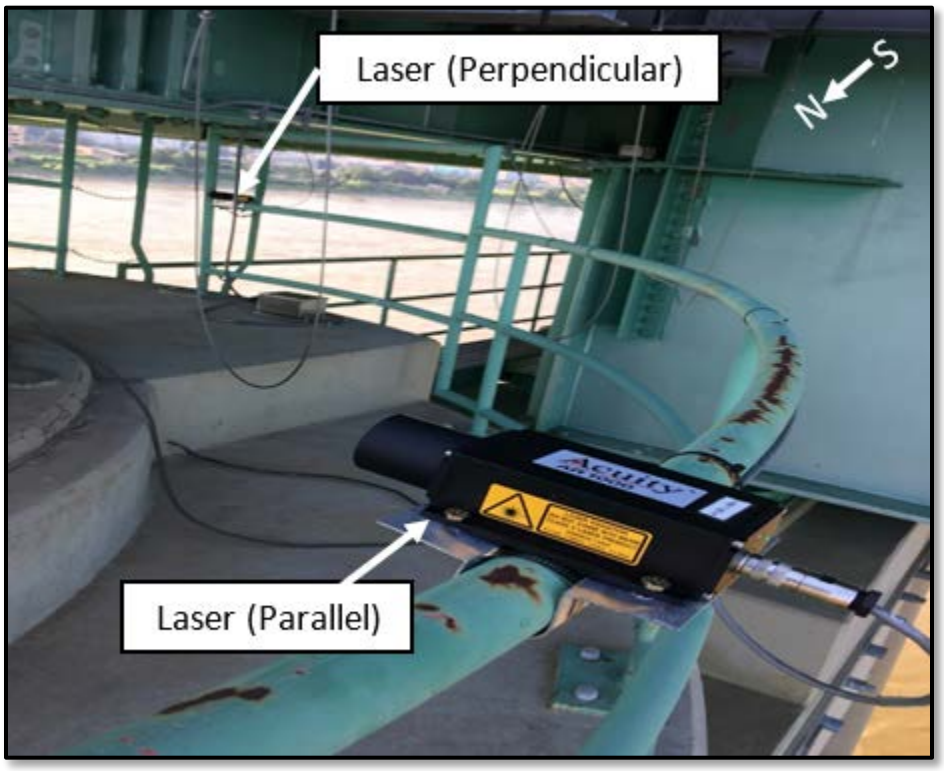

Figure 6.10 - Laser Orientation on Pier Cap

CHAPTER 7

DATA PROCESSING AND INTERPRETATION

The third objective of this project was to collect and analyze the data in order to determine the current performance of the bearings at Pier A and Pier C, determine the force distribution in the members framing into these bearings, and provide a framework with threshold criteria for the future automated SHM system. In order to accomplish this objective, data was collected over the span of three months from the Hernando DeSoto Bridge SHM system and uploaded into MATLAB where a program was developed to process and analyze the data. With the use of this program, the current bearing performance was analyzed at both Pier A and Pier C, the force distribution in the members framing into the bearings was determined, and percentages of the theoretical movement were calculated. The results from the analysis at each pier are described separately below.

7.1 Pier A Evaluation

7.1.1 Data Organization

The first step to process the raw data for it to be analyzed was to zero it. In order to zero the data, a reading of all the gages at a time where the bridge was at a steady state was chosen through studying the data. These values were then subtracted from every reading. For the structure to be at a steady state, the temperature was stable with minimal temperature gradients throughout. This allowed for consistent deviations in the measured responses during the data interpretation. Once zeroed, different relationships were analyzed and studied to understand the movements in the bearings and the response the bridge had to temperature changes throughout a typical day.

The second step was to investigate different relationships in the data in order to study the behavior of movement experienced in the bearings. Displacement versus temperature graphs were developed within the MATLAB program to understand and quantify how much the bridge is expanding and contracting when it heats up and cools down during a typical day. Before graphing this relationship, the temperature readings from each thermistor along Pier A were averaged at every sampling interval to develop an average temperature at Pier A. This allowed the data to represent the average temperature at Pier A in its entirety and not just at one particular location. While studying the bearing displacement and temperature relationship at Pier A, a cyclic pattern was discovered as the

bridge heated up during the day and cooled down at night. This cyclical pattern can be seen over a one day period, a two day period, and a three day period in Figure 7.1.

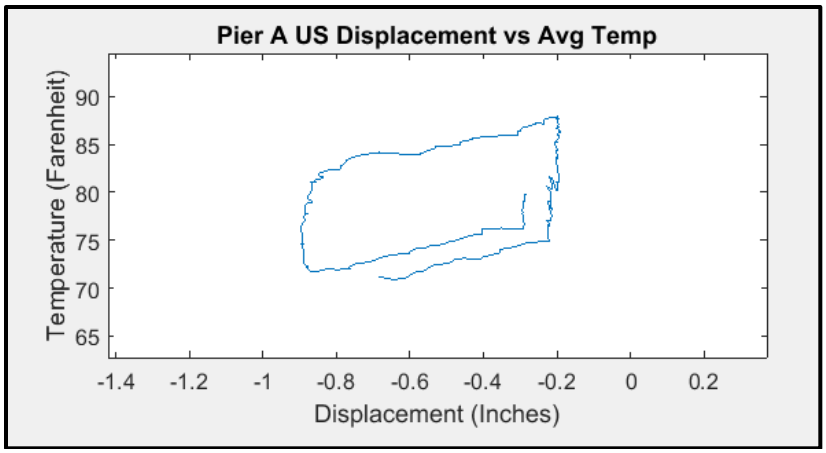

(a)

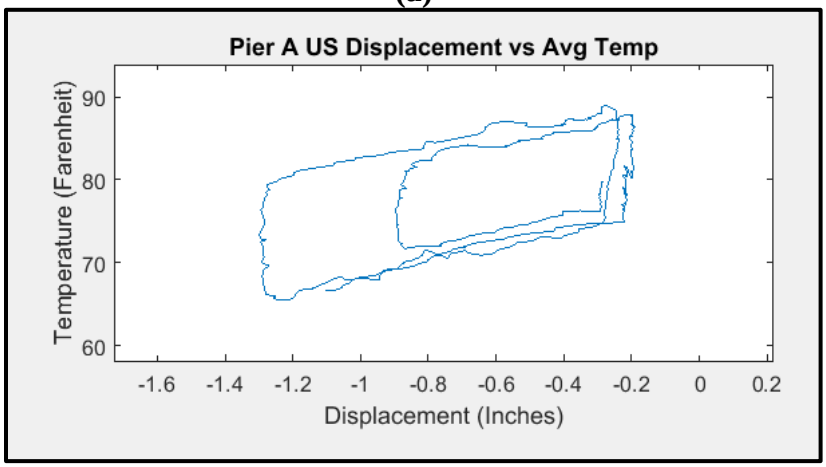

(b)

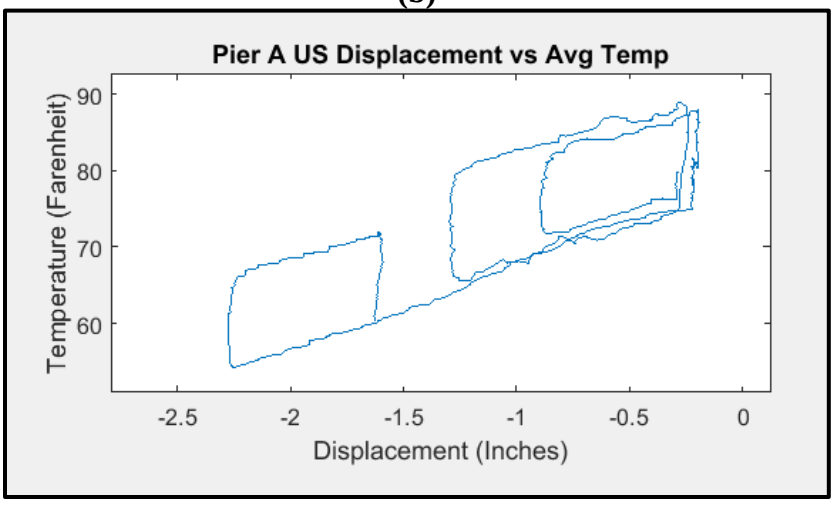

(c)

Figure 7.1 – Bearing Displacement vs. Temperature over October 6 (a), October 6-7 (b), and October 6-8 (c), 2016

Upon discovery of this pattern, significant effort was devoted for understanding the bridge's response to temperature changes throughout the day, and specifically what each portion of the graph represented. During the mornings as the sun begins to rise, the temperature increases, and the bridge structure begins to heat up. This increase in temperature causes the bridge to thermally expand as the materials that make up the structure begin to thermally expand. Frictional forces within the friction pendulum bearings prohibit the bridge from expanding causing a semi-vertical line to appear in the bearing displacement versus temperature graphs. This is because movement within the bearings will not occur until the summation of the horizontal forces in the members due to thermal expansion exceeds the frictional force within the bearings. For explanation purposes, this semi-vertical line that represents minimal displacement during increasing temperature readings will be called the "early stick". The early stick section of the graph is circled in Figure 7.2.

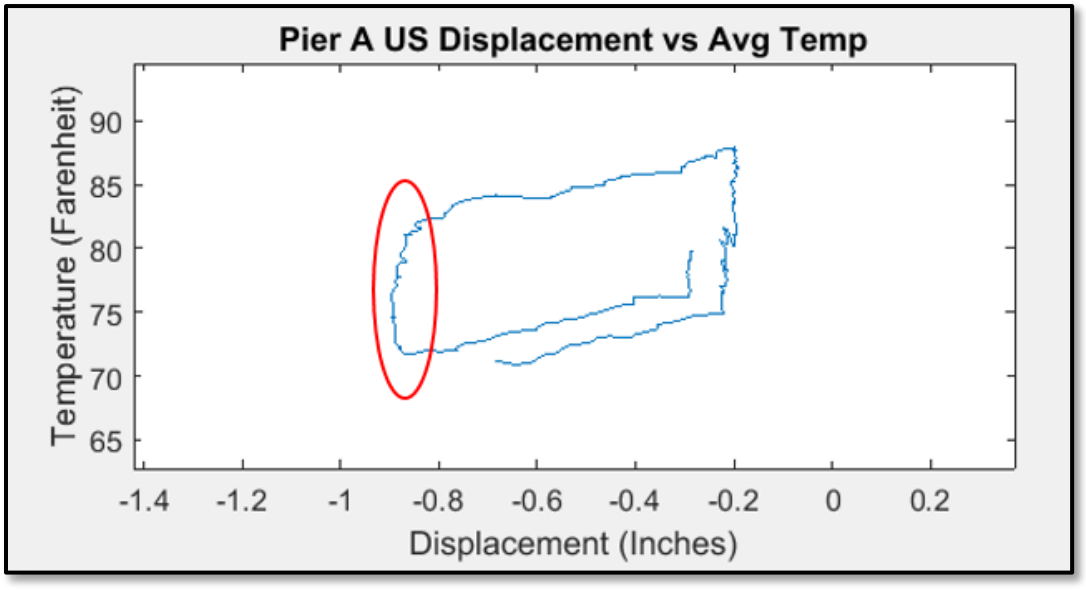

Figure 7.2 - Early Stick

Once the horizontal forces in the members exceed the frictional force within the bearings, the bridge begins to move, and the displacement begins to increase as temperature increases. The bridge will continue to displace until the force build-up in the members ceases to exceed friction. This halt in displacement happens when the temperature begins to decrease causing a lack of member force build-up. Similarly, due to this decrease in temperature, a semi-vertical line is also produced in the bearing displacement versus temperature relationship. As the temperature decreases, the bridge structure begins to try to shrink but is initially not able to due to the friction in the bearings. Not until the forces in the members due to shrinkage exceed friction can the bridge begin to contract. This period of time where there is minimal displacement while temperatures decrease will be called the "late stick". The late stick section of the graph is circled in Figure 7.3.

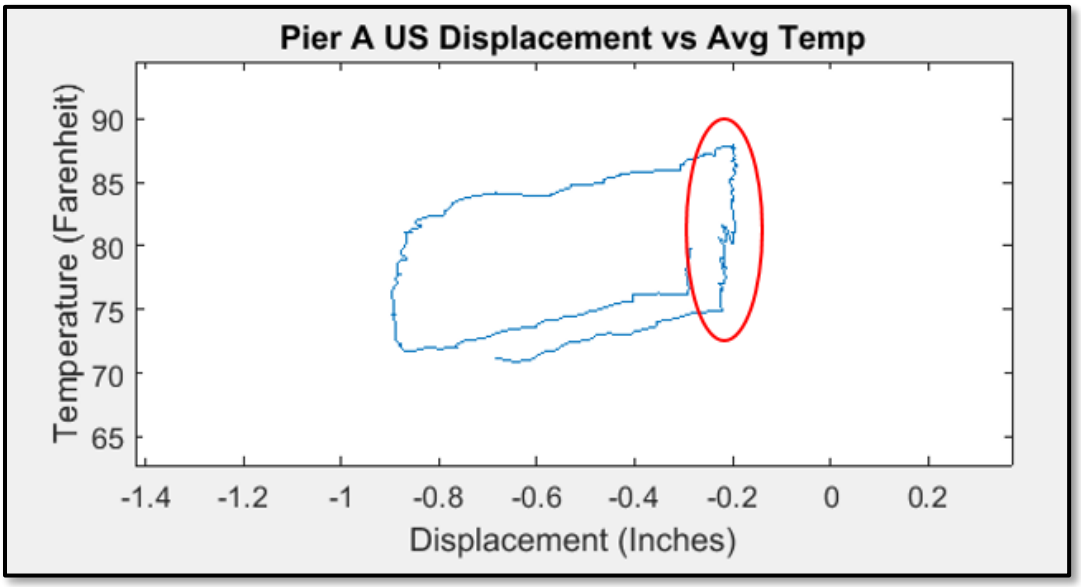

Figure 7.3 - Late Stick

Using the member strains during the early and late stick time periods, the member force distribution can be determined, and the coefficient of friction within the bearings can be calculated in order to evaluate the bearing performance at Pier A.

7.1.2 Data Selection

In order to determine the force distribution in the members framing into the bearings at Pier A and to evaluate the bearing performance by back calculation of the coefficient of friction, the change in member strains during the early and late stick times had to be captured. This change in strains represented the force needed to break friction which can then be used to determine the coefficient of friction in the bearings. However not all the days collected over the 3 month span could be used. Specific days and times had to be selected in order to 1) capture the structure at a steady state to reduce out-of-plane bending effects and 2) capture the structure during a period of time where lateral temperature gradients were minimal. Since two strain gages were attached to each member, the average of their responses was used to compute the axial strain neglecting in-plane bending. Nevertheless, this calculation was not sufficient to neglect out-of-plane bending effects. Therefore, different strategies had to be developed in order to select the days that provided the most reliable data in computing axial strain.

Lateral temperature gradients can be created when one particular side of the bridge is exposed to more direct sunlight than the other. This exposure to direct sunlight can cause

members to have one side heat up faster causing out-of-plane bending to occur. Because the strain gages were attached to the roadway side of the members, strains due to out-of-plane bending were captured in the strain data in addition to the axial member strains. This became a challenge due to the fact that there was no logical way of determining how much of the measured member strains were caused by out-of-plane bending with the system implemented on the structure. Initially, the strain gages were designed to be attached to the inside faces of the built-up members, but there was no access for the gages to be placed on the inner part of the members. Moving forward, it became paramount to try to minimize the influence out-of-plane bending had on the strain data by specifically selecting certain days with certain criteria that would allow the strain measured to be predominantly axial.

First, in order to minimize the out-of-plane bending in the members, days that were predominantly cloudy were selected due to the lack of direct sunlight the structure experienced. By looking at the local weather history in Memphis, Tennessee, different cloudy days were selected to be analyzed. What was discovered was due to the lack of temperature change during some cloudy days, the member force build-up was insufficient to break friction causing no appearance of the early stick or late stick times. Without the early and late sticks, the frictional force in the bearings could not be determined since the member force build-up never exceeded friction. Because there were not an abundance of predominantly cloudy days during the data collection period where the forces of friction were exceeded, additional days had to be selected in order to have enough data to evaluate the bearing performance.

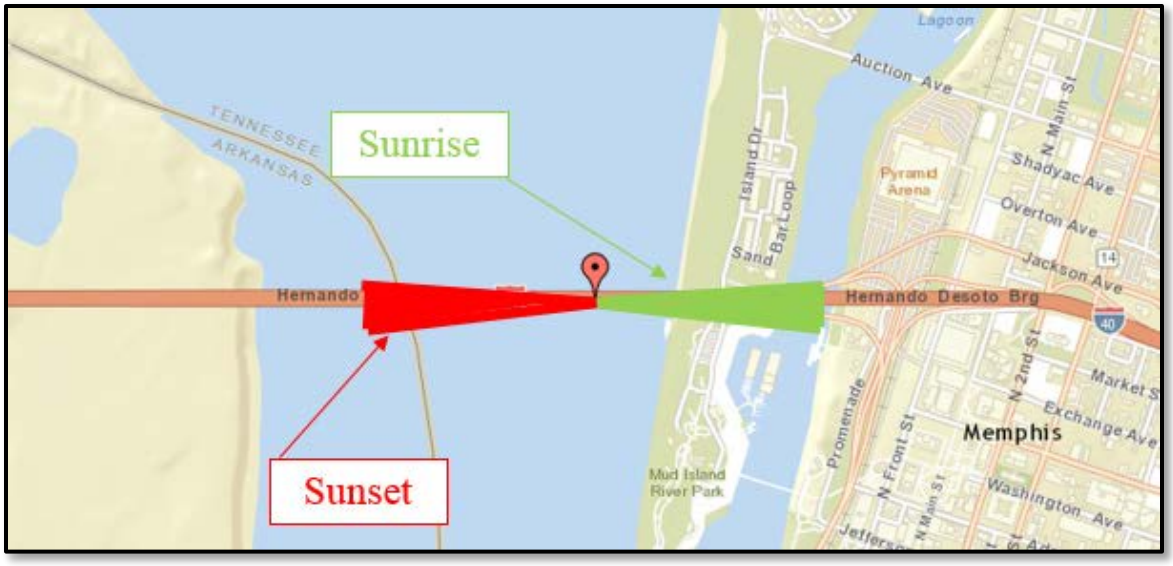

Figure 7.4 - Sun Positioning Envelope

Sun positioning during the collection period was investigated. Using the National Oceanic and Atmospheric Administration (NOAA) sun position calculator, sunny days where the sun's positioning throughout the day was close to directly over the bridge structure were found and used. An envelope showing the sun's positional relative to the Hernando DeSoto Bridge during the selected days can be seen in Figure 7.4. The time period selected to provide the best quality of data was September 17th - October 8th, 2016. The sun positioned over the bridge throughout the day would suggest longitudinal temperature gradients were produced and not lateral temperature gradients because one side of the bridge would not be exposed to more sunlight than the other. This reasoning would allow for the inclusion of certain sunny days since it also minimized the lateral temperature gradients produced by the position of the sun. Longitudinal temperature gradients produce axial thermal expansion which would minimize any out-of-plane bending occurring in the members and allow the strain readings to be mainly axial strains. With these specifically chosen days, their early and late stick time frames were used to

capture the change in strains and determine the force distribution in the framing arch members of the upstream and downstream bearings at Pier A.

7.1.3 Member Force Distribution

To begin analyzing the data from the selected days, the time frame for the early stick and late stick times had to be determined. These time frames were picked by selecting the gage readings from right before the early and late sticks occurred in the displacement versus temperature graphs and the gage reading right after each stick occurred where the forces in the bearings broke friction. Once these time frames were determined, the strain versus average temperature graphs were developed for each member framing into the bearings. A display of one of the temperature versus strain graphs for the members framing into the upstream bearing on Pier A during the early stick time frame is shown in Figure 7.5.

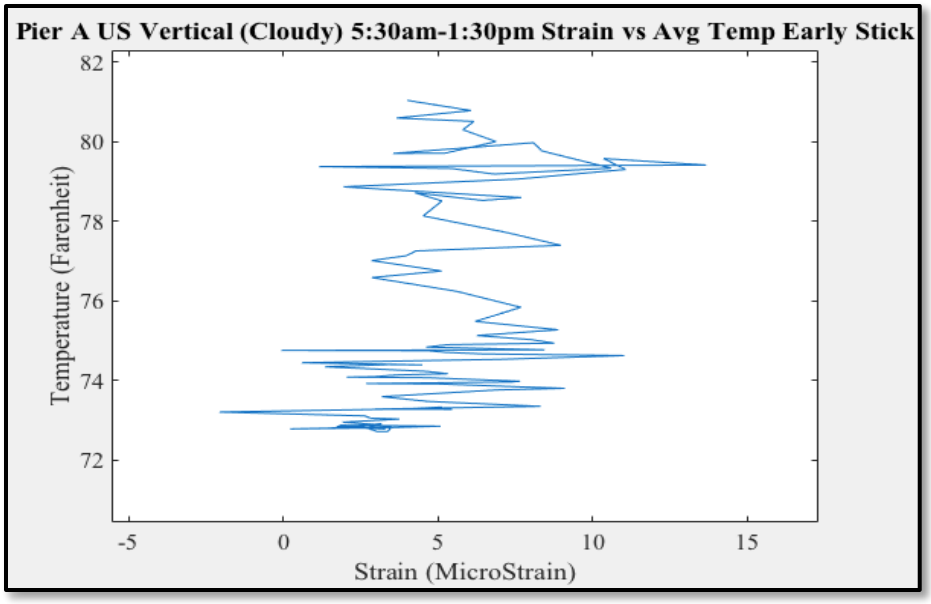
Pier A US Vertical (Cloudy) 5:30am-1:30pm Strain vs Avg Temp Early Stick
Temperature (Farenheit)
82
80
78
76
74
72
-5
0
5
10
15
Strain (MicroStrain)

(a)

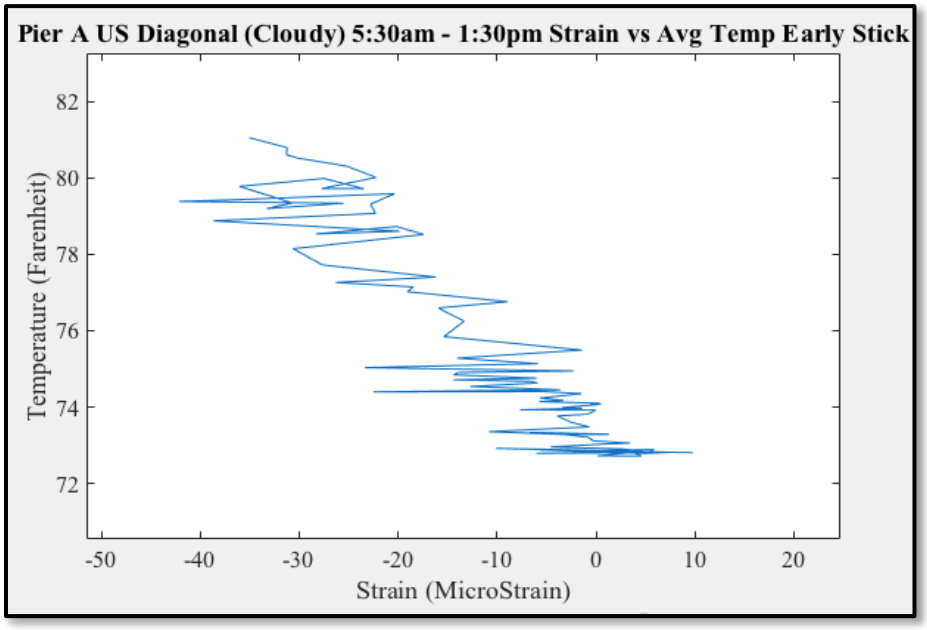
Pier A US Diagonal (Cloudy) 5:30am - 1:30pm Strain vs Avg Temp Early Stick
Temperature (Farenheit)
82
80
78
76
74
72
-50
-40
-30
-20
-10
0
10
20
Strain (MicroStrain)

(b)

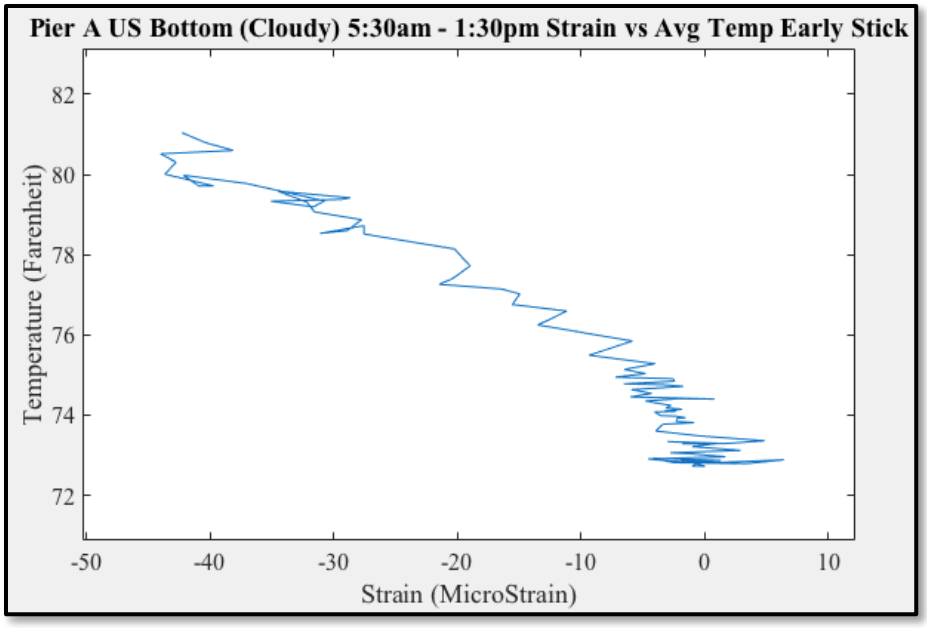

(c)

Figure 7.5 - Vertical (a), Diagonal (b), and Horizontal (c) Member Temperature vs. Strain Graphs

Using these relationships, the change in strains were determined for each member framing into each bearing as they relate to the frictional force experienced in the bearings. With the assumption that there was minimal out-of-plane bending and that all the strains measured were due to axial force and in-plane bending, the strain values were converted into stresses using Hooke's Law shown in Equation 2.

$$\sigma = E\varepsilon \qquad \textbf{Eq. 2}$$

where, σ = stress in members

E = modulus of elasticity for steel

ε = measured strain in members

With the modulus of elasticity for steel (E) to be 29,000 ksi, the measured strain (ε) was multiplied by the modulus of elasticity for steel to determine the stress (σ) experienced in

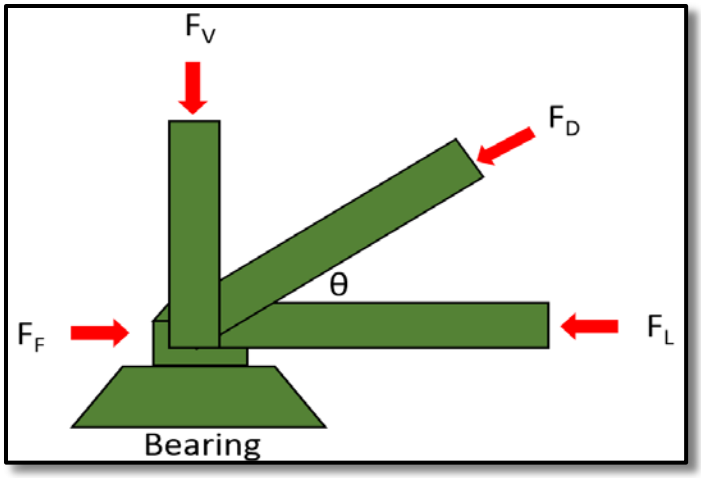

Figure 7.6 - Free Body Diagram of Arch Members Framing into the Bearings

the members during each early and late stick. The calculated stress values were multiplied by the cross-sectional area of the members found in the plans provided by TDOT to calculate the axial forces in the members. A free body diagram of the force distribution in the arch members framing into the bearings is shown in Figure 7.6. Using equilibrium, the assumption of no shear forces in the vertical members, and ignoring the minimal influence the small curvature of the bearing base plate has since temperature movements occur at the center of the bearing as opposed to the edges, forces were summed in the horizontal direction to identify the frictional force in each bearing (F_F) as shown in Eq. 3.

$$F_F = F_L + F_D \cos\theta \qquad \textbf{Eq. 3}$$

where, F_L = force in lower chord

F_D = force in diagonal chord

θ = angle between diagonal and lower chords

Table 7.1 - Pier A Early and Late Stick Friction Force Results

Upstream Bearing		
Time Frame	**Early stick**	**Late Stick**
Frictional Force Range (kips)	173.1-251.1	192.3-259.7
Frictional Force Mean (kips)	211.2	224.1
Frictional Force Standard Deviation	22.2	18.0
Downstream Bearing		
Time Frame	**Early stick**	**Late Stick**
Frictional Force Range (kips)	160.8-265.4	155.4-336.8
Frictional Force Mean (kips)	205.4	274.9
Frictional Force Standard Deviation	32.7	34.4

The results of the measured friction force experienced during the early and late stick time frames in the bearings at Pier A is shown in Table 7.1. Along with the calculated average friction force, a standard deviation was performed for each bearing to provide insight as to how much the measured friction forces varied during the selected time period.

7.1.4 Coefficient of Friction

The final step to evaluating the bearing performance at Pier A was to calculate the coefficient of friction in the friction pendulum bearings and compare the measured values to the design values. An estimated dead load on the bearings from the bridge plans provided by TDOT was 4022 kips. The coefficient of friction (μ_F) was calculated using the friction force values from the analyzed early and late stick time frames (see **Error! Reference source not found.**).The equation used to determine the coefficient of friction is shown in Equation 4.

$$\mu_F = \frac{F_F}{F_{DL}} \qquad \textbf{Eq. 4}$$

where, μ_F = Coefficient of Friction

F_F = Frictional Force

F_{DL} = Estimated Dead Load

The coefficient of friction values were averaged, and a standard deviation was performed to display the accuracy of the values collected from the data. These values along with the mean coefficient of friction values can be seen in Table 7.2.

Table 7.2 - Pier A Bearing Performance Values

Pier A Bearing Performance Values		
Bearing	**Upstream Bearing**	**Downstream Bearing**
Coefficient of Friction Range	0.04-0.06	0.04-0.08
Mean of Calculated Coefficient of Friction	0.05	0.06
Standard Deviation of Coefficient of Fricition	0.0063	0.0122

7.1.5 Percentage of Movement at Pier A

To compare the theoretical movements to the measured movements in the bearings at Pier A, a linear regression analysis was performed using the displacement data. Because the long-term slope of the displacement versus temperature data could be best determined by a line of best-fit, linear regression analysis was considered sufficient. The theoretical longitudinal movement at Pier A was calculated using the equation for linear thermal expansion which is shown in Equation 1. This linear regression analysis technique was also applied by Yarnold, Dubbs [15], Herman, Helwig [18], and Wang, G., el. al. [19].

Based on the data collected over a three-month period, a linear regression was performed on each bearing to create a line of best-fit through the displacement versus temperature data. The slope of the line of best-fit was used to determine the amount of movement seen per degree of temperature change. The linear regression performed on each bearing data can be seen in Figure 7.7and Figure 7.8.

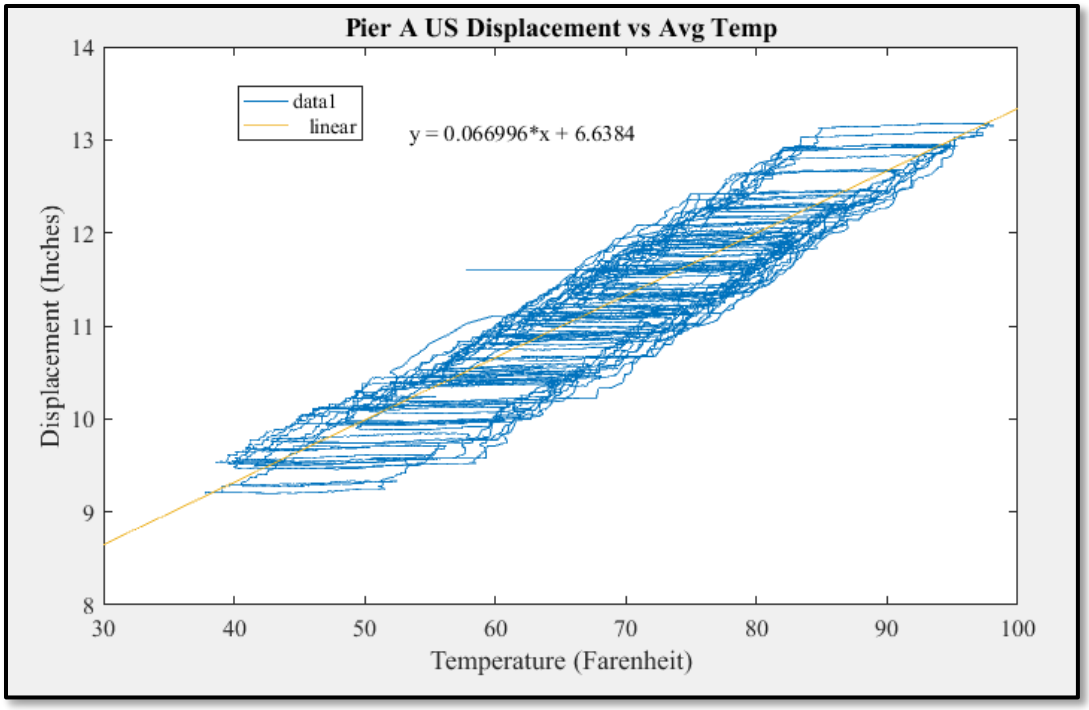

Figure 7.7 - Pier A Upstream Bearing Data

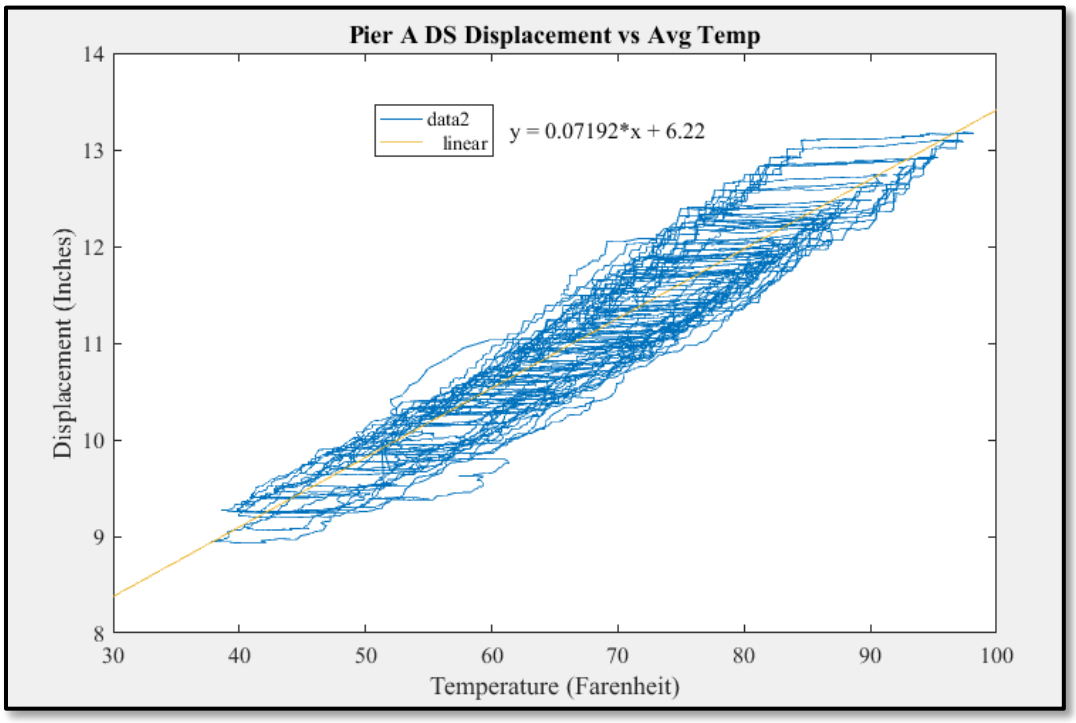

Figure 7.8 - Pier A Downstream Bearing Data

With the assumption that the thermal neutral point occurred at Pier B due to the structure's symmetry, the average of the change in temperature at Pier A and Pier C over the three months was used, and a slope of the theoretical movement of $0.0702\frac{in}{°F}$ was calculated. The slope of the theoretical movement was computed using Equation 5.

$$Slope = \frac{\delta}{\Delta T} = \alpha L \qquad \textbf{Eq. 5}$$

where, α = coefficient of thermal expansion of steel
ΔT = uniform change in temperature
δ = change in length
L = span length

The evaluated reciprocal of the slope for the upstream and downstream bearings were $0.067\frac{in}{°F}$ and $0.072\frac{in}{°F}$. This was roughly 95% and 103% of the calculated theoretical movement, respectively. The small difference in movement could be equated to flexure occurring in the substructure at Pier A. In addition, the difference could be a result of the coefficient of thermal expansion being slightly higher than estimated. In either case, the bearings at Pier A illustrate sufficient movement with temperature change.

7.1.6 Pier A Bearing Performance Summary

The friction pendulum bearings at Pier A were studied and evaluated thoroughly over a course of three months indicating adequate performance levels. Based on the

calculated data in this study, the coefficient of friction in the downstream bearing roughly matched the design values provided in the plans, and the upstream bearing had a value slightly lower than its design value. In addition, the percentage of displacement measured at the Pier A bearings compared to the theoretical movement was reasonable, indicating adequate thermal movement. In conclusion, the comparison performed in this study between measured and theoretical movement experienced in the Pier A bearings validates proper functionality.

7.2 Pier C Evaluation

7.2.1 Analyzing Bearing Movement

The data collected over the three-month period was processed and analyzed through the exact process performed to Pier A. The process of organizing and selecting the data can be reviewed in sections 7.1.1 and 7.1.2 in this thesis. Over time, challenges arose in acquiring data from Pier C due to the frequency interference the city of Memphis had on the system. Data sent from Pier C to the main setup at Pier A was being interfered which caused gaps in the data. This interference did not affect the quality of the data, but it affected the quantity of data retrieved from the system. To overcome this challenge, the data was scrutinized in order to select time frames within the time frames established

during the data selection process described in section 7.1.2 that produced reliable data with minimal data interferences.

The displacement versus temperature graphs displayed limited movement measured at Pier C compared to the movements measured at Pier A. Some movement was captured as temperatures dropped toward freezing during the later months of the fall season. The displacement versus temperature graphs of the Pier C upstream and downstream bearings illustrating the movement captured over the collection period can be seen in Figure 7.9 and Figure 7.10.

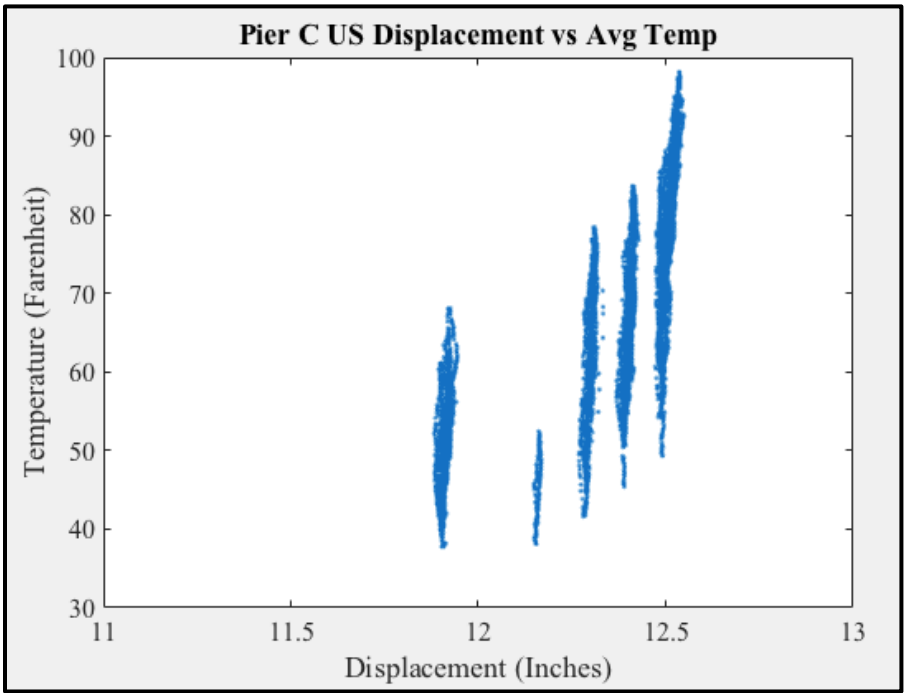

Figure 7.9 - Pier C Upstream Bearing Displacement vs. Temperature

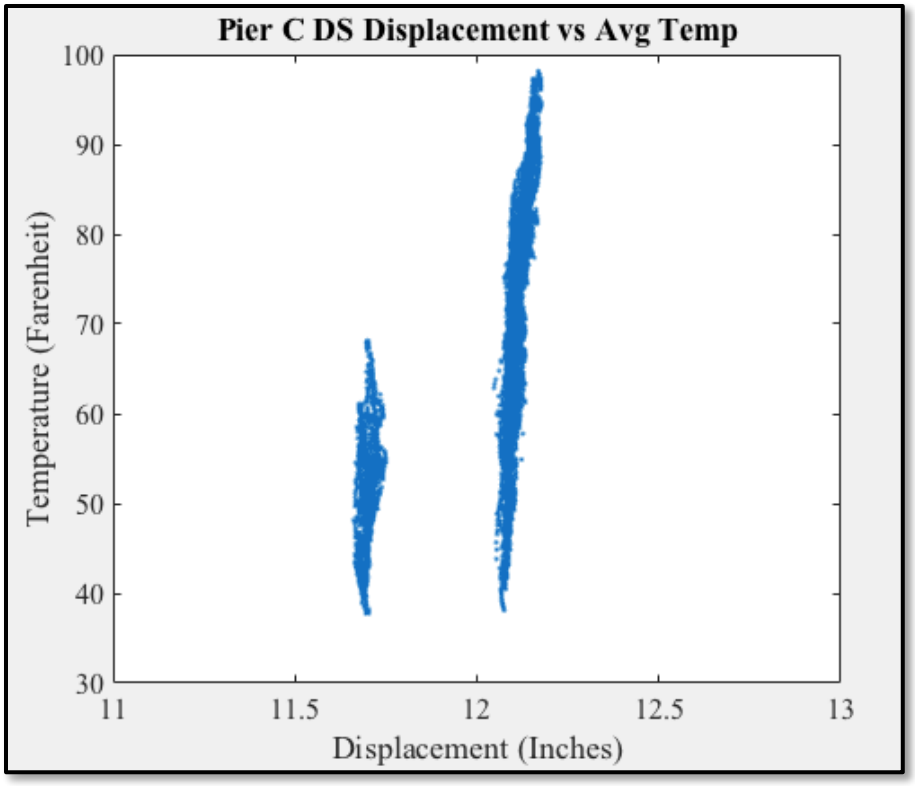

Figure 7.10 - Pier C Downstream Bearing Displacement vs. Temperature

To understand the difference in the measured movement at Pier A and Pier C, a time-history plot of the displacements experienced at Pier A and Pier C is shown in Figure 7.11. Based on the figure shown below, there is a significant difference in the amount of displacement measured at each pier.

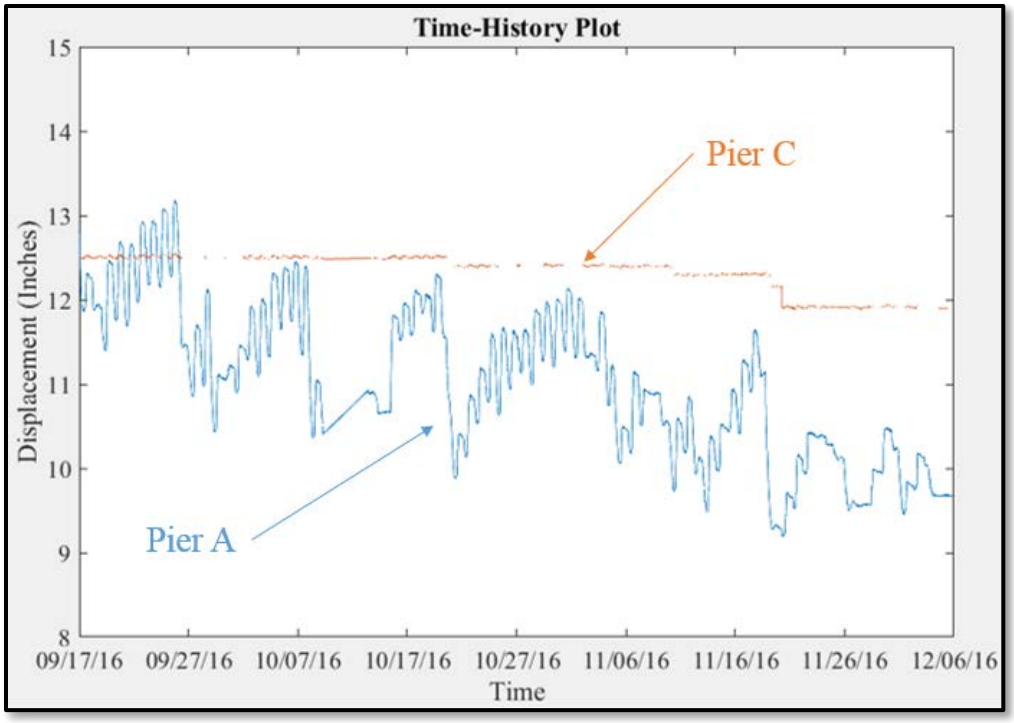

Figure 7.11 - Pier A and C Comparison Time-History Plot

Upon this discovery, quality control checks were performed to ensure the readings were accurately representing the movement captured at Pier C. The code was checked multiple times to ensure the displacement gages were measuring the displacements correctly and in the units that were desired. An installation check was performed on all the wiring and mounting of the displacement gages, and readings from both gages were compared to provide redundancy to what was being measured.

Once the data was deemed accurate, member strains at Pier C during the late stick time frames established for Pier A were graphed versus temperature. Early stick and late stick time frames for the bearings at Pier C could not be determined since no cyclical movement was seen. The best alternative was to look at the strains during the late stick time frame established by the Pier A bearing movements. The strains measured at Pier C

Table 7.3 - Late Stick Friction Forces

Late Stick Friction Force		
Pier A		
Member	Diagonal Chord	Bottom Chord
Average Δ Strain	62.2	79.0
Average Stress (ksi)	1.8	2.3
Average Horizontal Force (kips)	250	
Pier C		
Member	Diagonal Chord	Bottom Chord
Average Δ Strain	48.9	70.1
Average Stress (ksi)	1.4	2.0
Average Horizontal Force (kips)	212	

and the horizontal force produced at Pier C due to thermal expansion were smaller than at Pier A which suggests that the force build-up in the members never exceeded friction. This comparison can be made since it is clear from the displacement versus temperature graphs that the forces at Pier A exceed friction during this time frame. Table 7.3 displays the average strain, average stress and average horizontal force experienced in each diagonal and bottom member at Pier A and Pier C during the established late stick time frame. The values calculated in Table 7.3 show a difference of 38 kips of force in the average horizontal force produced by the member strains. By multiplying the designed dead load of 4022 kips and the designed coefficient of friction of 6%, the force build-up needed to break friction is roughly 241 kips. The average horizontal force measured in the bearings at Pier C is 212 kips. This is approximately 12% less than the required force needed to break friction in the bearings. This lack of force build-up in the members at Pier C during a time frame that should experience bearing movement may indicate the expected thermal movement is occurring at another location of the bridge.

The investigation of the bearings at Pier C shows that the force build-up in the instrumented members does not exceed the friction in the bearings. This verifies why limited movement was measured at Pier C. A comparison of the measured movement with the theoretical movement was not necessary based on the obvious limited movement described above. Theories as to where the movement was distributed were developed and presented to TDOT.

7.2.2 Theories Behind Limited Bearing Movement at Pier C

The initial theory to explain the lack of movement measured at Pier C was that the bearings were locked up, but through further investigation, this theory was considered false. If the bearings were locked up or "frozen", a substantial amount of force build-up would be measured in the instrumented members. In theory, there should be close to the same amount of movement occurring at Pier C as there is at Pier A. Not only was there no substantial strain build-up in the members at Pier C, but in fact the strains were less than the measured strains at Pier A. If member forces never exceed friction, no movement will occur in the bearings.

Another theory as to why the Pier C bearings measured limited movement was gage malfunction. This was investigated through numerous quality control checks. Even with rigorous quality control checks, it was realized that there is always a possibility of the measured data to be false readings, but pictures taken during installation were reviewed to

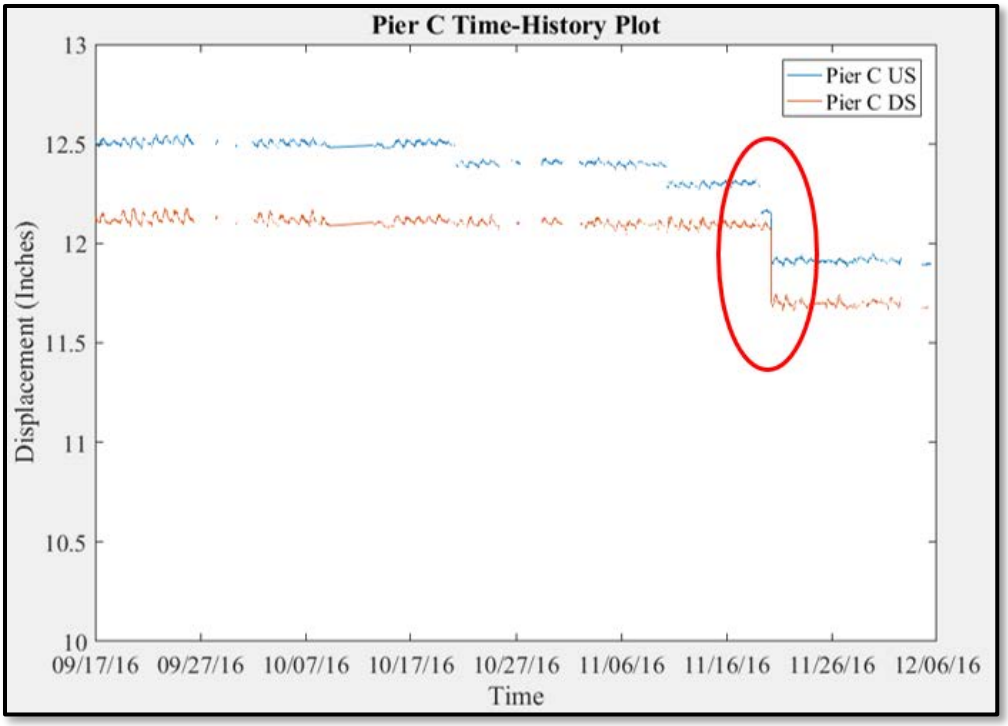

Figure 7.12 - Maximum Captured Movement at Pier C Bearings

determine if any details in the attachment process would alter the data. This theory was doubtful due to the redundancy of the measurements measured by both displacement gages, and as temperatures dropped significantly at the end of the three-month period, movement was seen in the bearings at Pier C. The maximum movement captured at the Pier C bearings is illustrated in Figure 7.12. Over the course of the data collection period, small amounts of movement were seen at the upstream bearing (blue line in Figure 7.12) at two instances previous to the instance the maximum displacement was captured. A maximum of roughly 0.4 inches was measured which suggests the displacement gages were working as designed since they are able to capture some movement.

Based on the lack of movement and force build-up measured at Pier C, the theory that the substructure at Pier C may be tilting was investigated. The lack of force or strain

Figure 7.13 - Substructure at Pier C

build-up in the members implies that the movement is occurring at another location on the bridge, which may be in the substructure. If the force needed to tilt the pier at Pier C is smaller than the force needed to exceed friction, the pier will tilt before any movement in the bearings occur. This movement in the substructure would explain the lack of force build-up in the members. A picture of the substructure at Pier C can be seen in Figure 7.13. Pier A and Pier C stand at 93 feet tall measuring from the footing to the top of the substructure. If the remaining theoretical thermal expansion movement occurred in the tilting of the substructure, it would produce a tilt angle of 0.19 degrees. This minute amount of tilt is invisible to the naked eye. In order to confirm this theory, a tilt meter would need to be implemented to the system to capture any tilt occurring in the substructure. Another option would be to use a non-contact displacement sensor with sufficient resolution to measure the global movement at the pier.

To add to the theory of the substructure tilting at Pier C, the different bridge approaches coming into Pier A and Pier C may have an effect on the pier's ability to tilt.

Pier A has an approach span much longer than the approach span at Pier C. The longer the approach span the greater the amount of thermal expansion will be which will produce a greater longitudinal force than the shorter span. The approach on Pier A also frames into friction pendulum bearings with a substantial amount of friction. The force produced by the combination of the expansion of the approach side of Pier A and the friction pendulum bearings would counteract the force produced by the thermal expansion of the bridge main section. The counteraction would keep the substructure at Pier A from tilting westward and would allow the displacement to be measured in the bearings. This may not be the case at Pier C since the approach is shorter and attached to the pier through lead-rubber bearings. The shorter approach may lack the ability to counteract the thermal expansion force occurring in the bridge's main section causing the substructure to tilt eastward. A diagram illustrating the concept of this theory is shown in Figure 7.14. As previously stated, the tilting of the substructure would

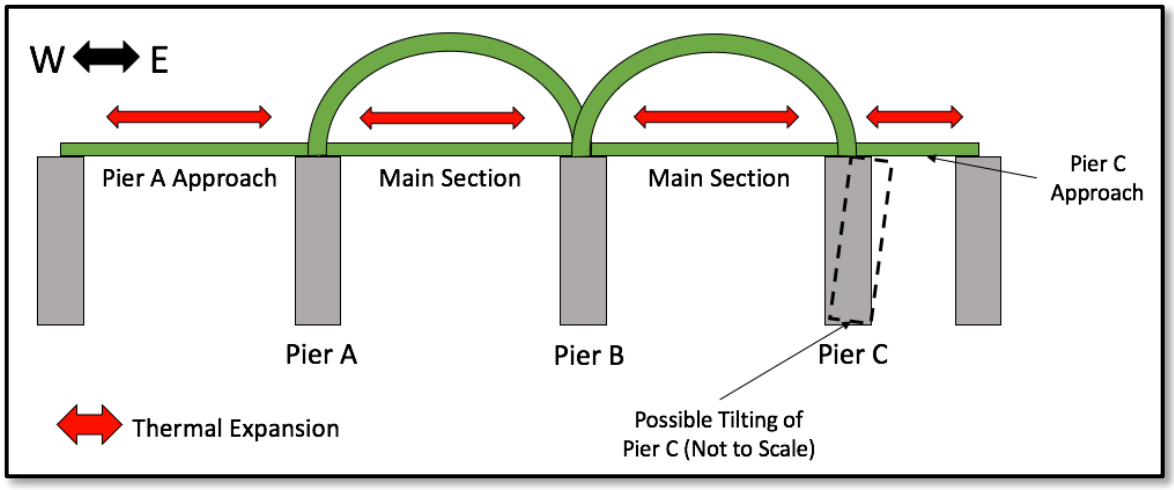

Figure 7.14 - Bridge Approach Illustration

explain the minimal movement measured in the bearings at Pier C and lack of strain build-up in the instrumented members.

7.2.3 Pier C Bearing Performance Summary

Displacement measurements at Pier C collected over a three-month period were processed and studied to determine the performance of the bearings. Through this study, limited movement was discovered at Pier C due to the lack of force build-up and inability to exceed friction in the arch members framing into the bearings. Because of the lack of movement measured at Pier C, bearing performance levels could not be determined. Several theories such as locked bearings, gage malfunction, and movement in the substructure were developed and investigated. The proposed theory is that the limited movement is due to substructure movement, however, no final conclusion was established. In addition, ideas were developed to upgrade the system implemented on the structure in order to validate whether the substructure is tilting. Ultimately the Pier C bearing performance could not be determined through field evaluation.

CHAPTER 8

LONG-TERM MONITORING

8.1 Real-Time Monitoring

The last objective was to develop a real-time monitoring display using a Campbell Scientific product called Real Time Monitor & Control Software (RTMC). An interface was developed to make an easy-to-use visual display that will allow TDOT and/or TTU to access the system and monitor the structure in real time. Basic alerting systems were also constructed within the interface with specific thresholds that were developed through months of data analysis. This interface with the implemented alerting systems will make monitoring the structure less tedious than looking through a table of numbers in LoggerNet.

The layout of the monitoring system interface first consists of an overview of the instrumentation showing the locations of each sensor on the south side of the structure. Note the instrumentation shown on the south side is completely symmetrical to the instrumentation on the north side of the structure. The overview page of the interface is shown in Figure 8.1.

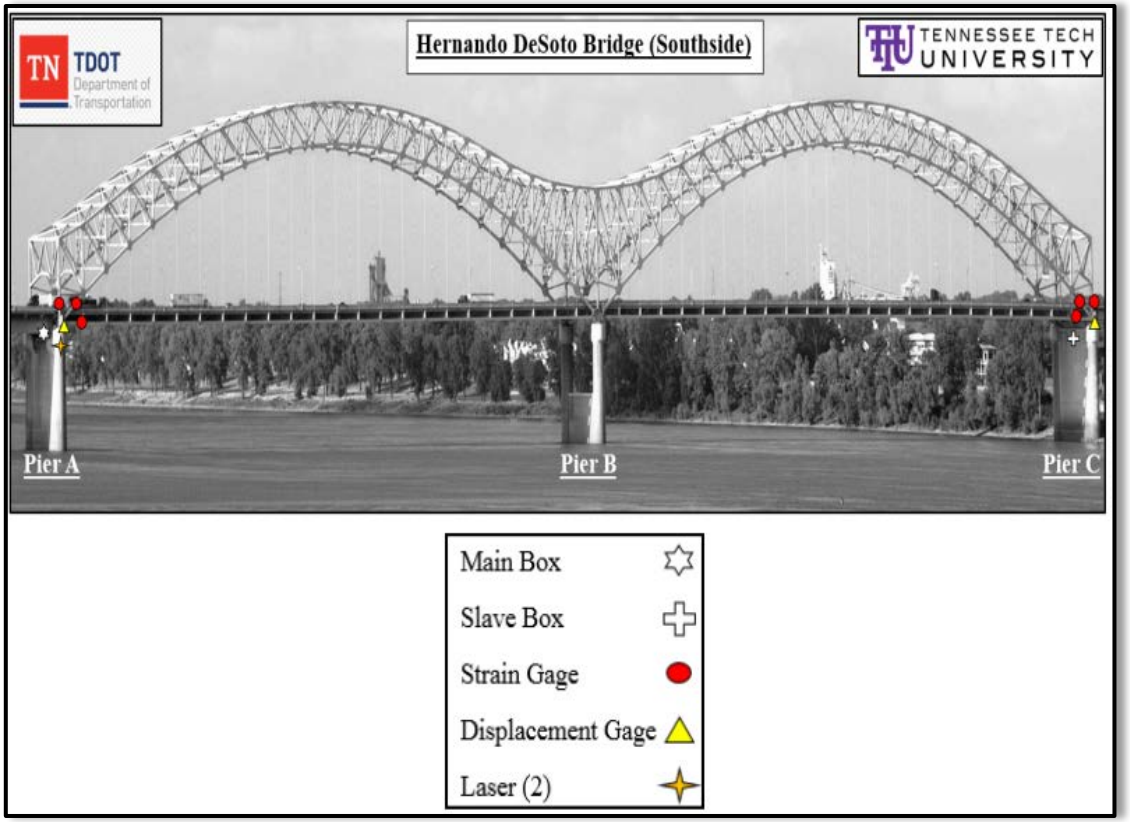

Figure 8.1 - Interface Overview Page

Figure 8.2 illustrates the time history plots for bearings displacements on Pier A and Pier C that were developed to monitoring the thermal movements of the structure. The Pier A and Pier C displacements displayed on this page represent zeroed measurements. More information on how the data was zeroed can be found in section 7.1.1. The top graph represents the bearing movements for the main section and approach bearing displacements at Pier A while the bottom graph represents the main section bearing displacement at Pier C. Along with the time history plots were displacement alarms to alert users of any anomalies or departures from normal bridge behavior in the bearing displacement readings. To determine the displacement thresholds for the alarms, a linear regression analysis was

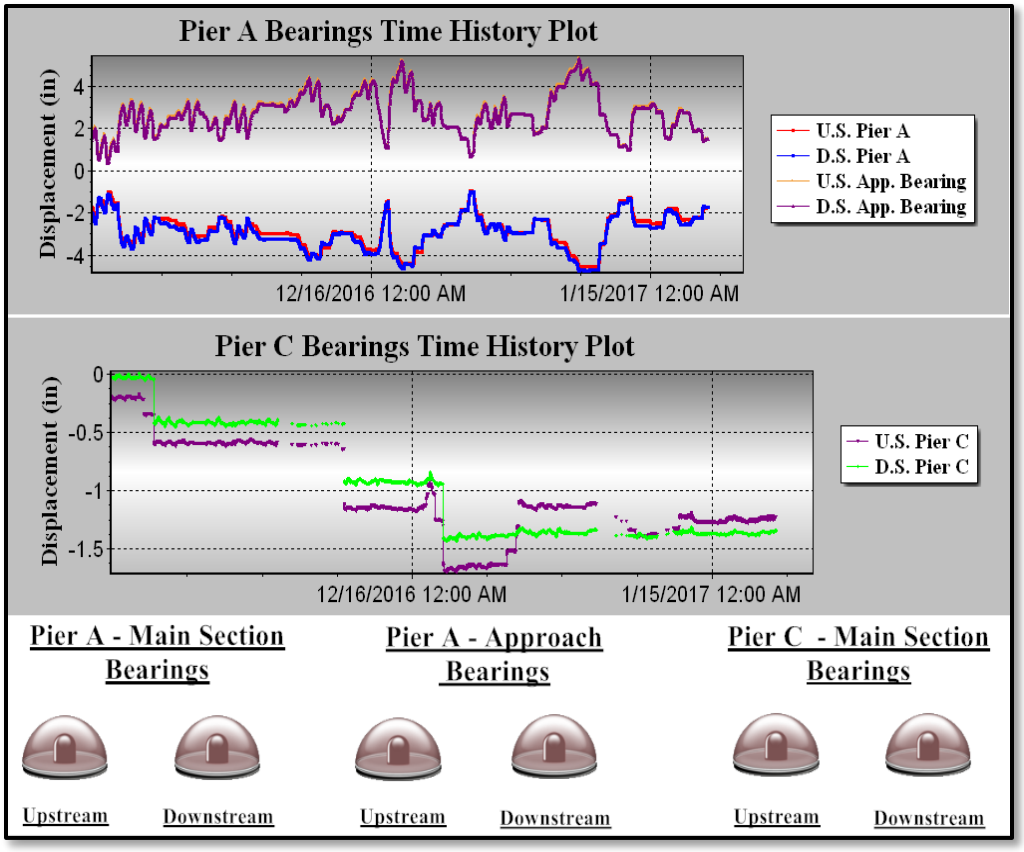

Figure 8.2 - Bearing Displacement Interface Time History Plots

performed on the displacement versus temperature graphs over the three-month period in MATLAB to extrapolate displacement values. The larger threshold was determined from the projected displacement at 120°F, and the smaller threshold was set to the projected displacement at 0°F.

In addition, strain time history plots and alarms were developed to display the change in strains throughout a typical time period. Strain values displayed on the interface were averaged and zeroed. The time history plots for the downstream strain readings for Pier A and Pier C are shown in Figure 8.3 and Figure 8.4, respectively.

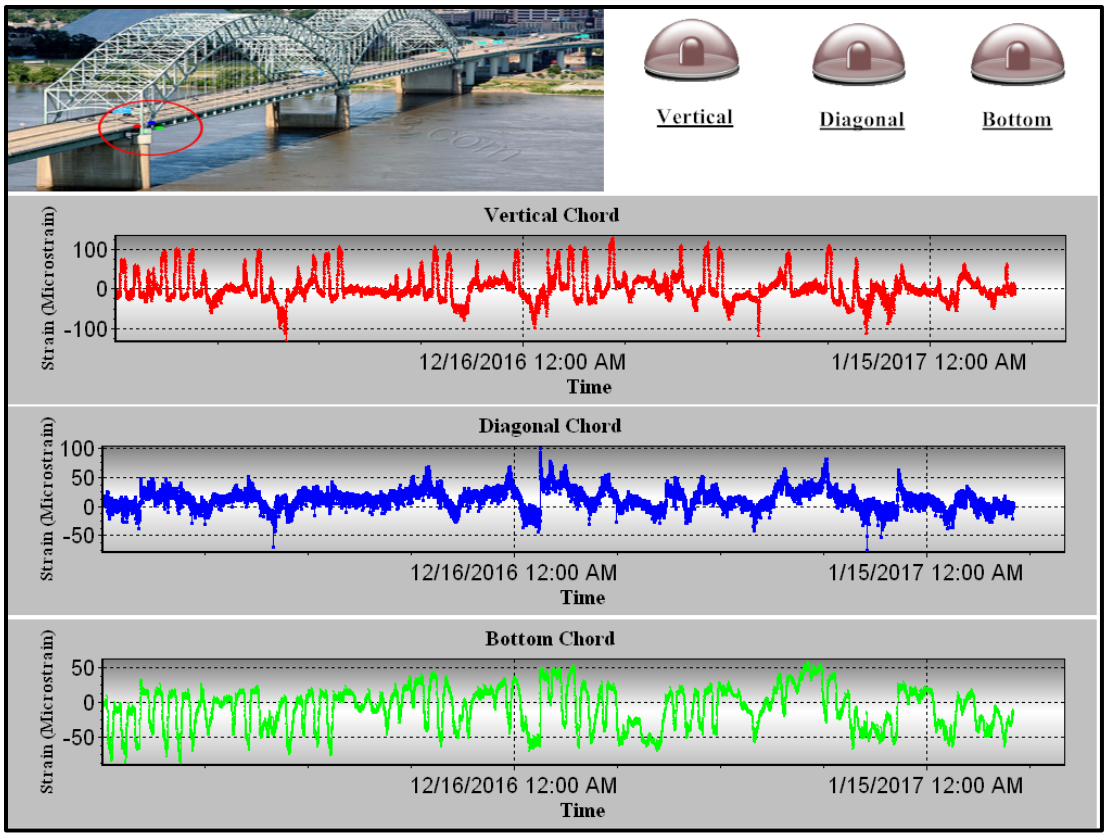

Figure 8.3 - Pier A Downstream Interface Strain Time History Plots

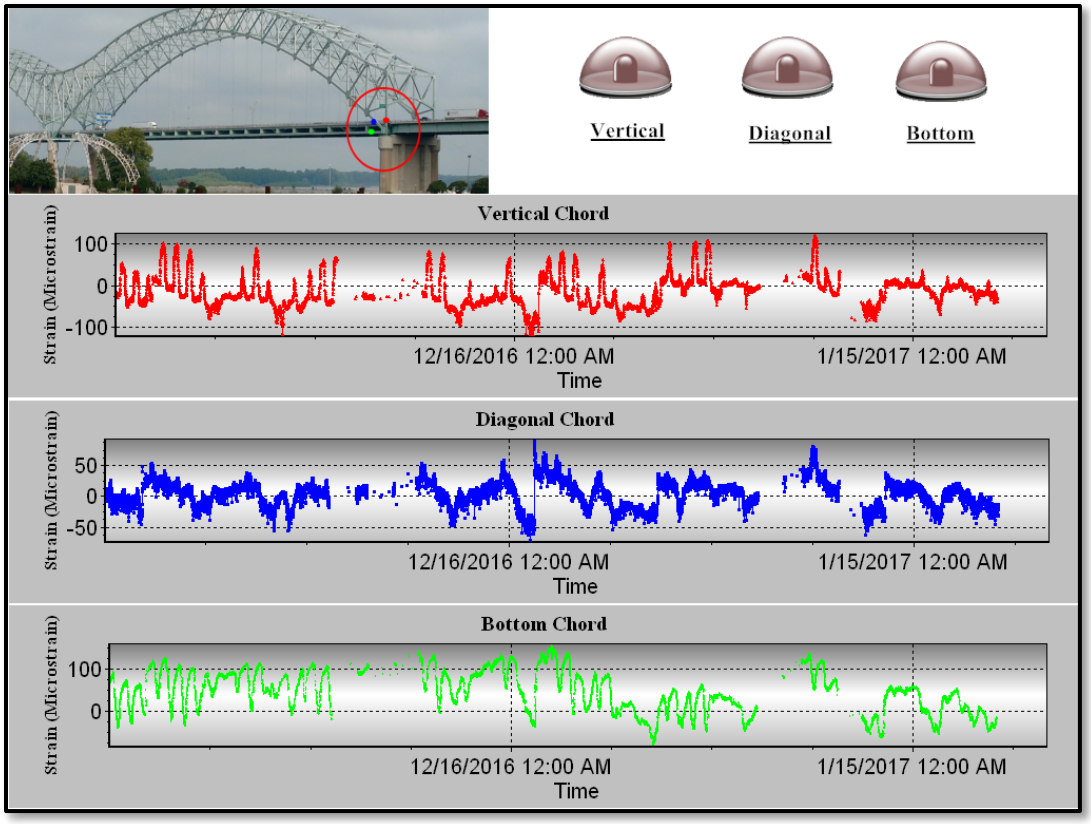

Figure 8.4 - Pier C Downstream Interface Strain Time History Plots

To determine the strain reading thresholds, the Pier A strain versus temperature relationships over the entire life of the monitoring system were examined. Using the tools in MATLAB, the maximum and minimum strain values captured over this period of time were ascertained in order to establish a foundation for the specific thresholds. Once acquired, the alarms were set with thresholds of 150% of what was measured for the maximum and minimum readings for each instrumented member. The displays for Pier A and Pier C include a picture showing the locations of the strain gages on the bridge with colored dots with color coordinated graphs that designate which gage the graph represents.

Following time history plots, displacement versus temperature relationships for Pier A and Pier C were developed. With this relationship implemented into the interface,

users will be able to see the cyclic pattern discussed earlier in this thesis and monitor the cyclic pattern to detect any changes to the natural movement occurring in the bearings. To have the displacement versus temperature relationship display the cyclic pattern, the displacement readings were zeroed, and the temperature readings were averaged. Figure 8.5 and Figure 8.6 illustrate the graphs for the upstream and downstream bearings at Pier A and Pier C along with a figure to specify the location of the bearings.

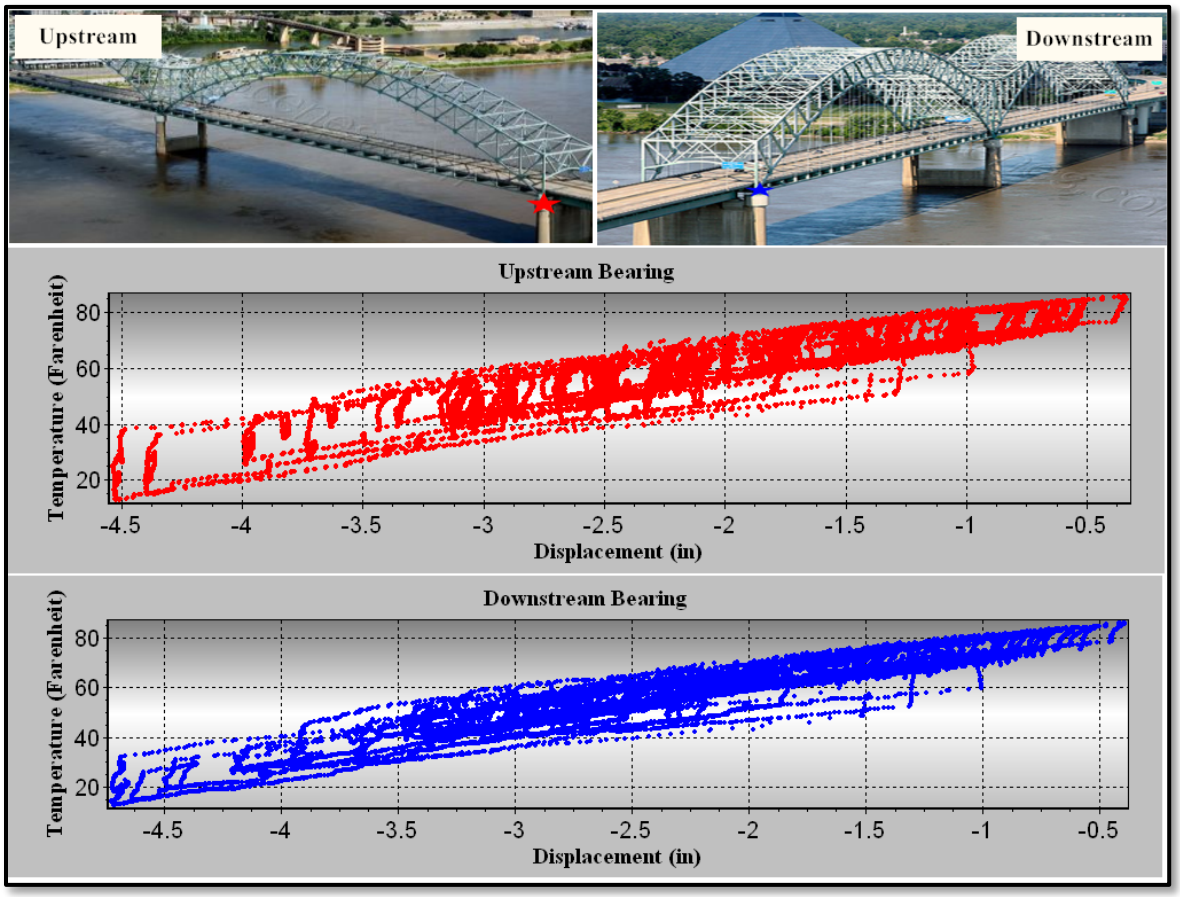

Figure 8.5 - Pier A Interface Displacement vs. Temperature Relationship

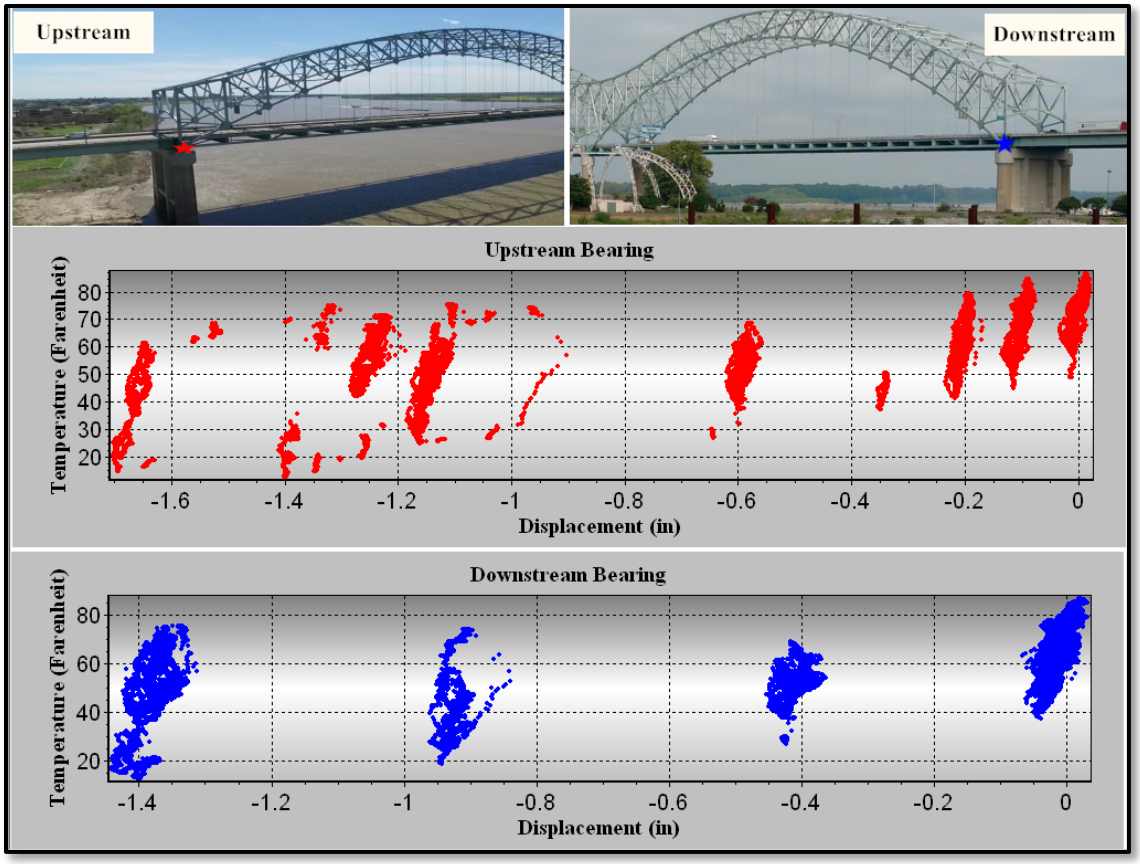

Figure 8.6 - Pier C Interface Displacement vs. Temperature Relationship

Laser readings for the seismic monitoring system were displayed in the real-time interface in order to monitor the bearing movements upon a seismic event. The graphs display the laser readings in feet along with alarms to alert users of substantial displacement and possible earthquake occurrence. The laser displacement graph can be seen in Figure 8.7.

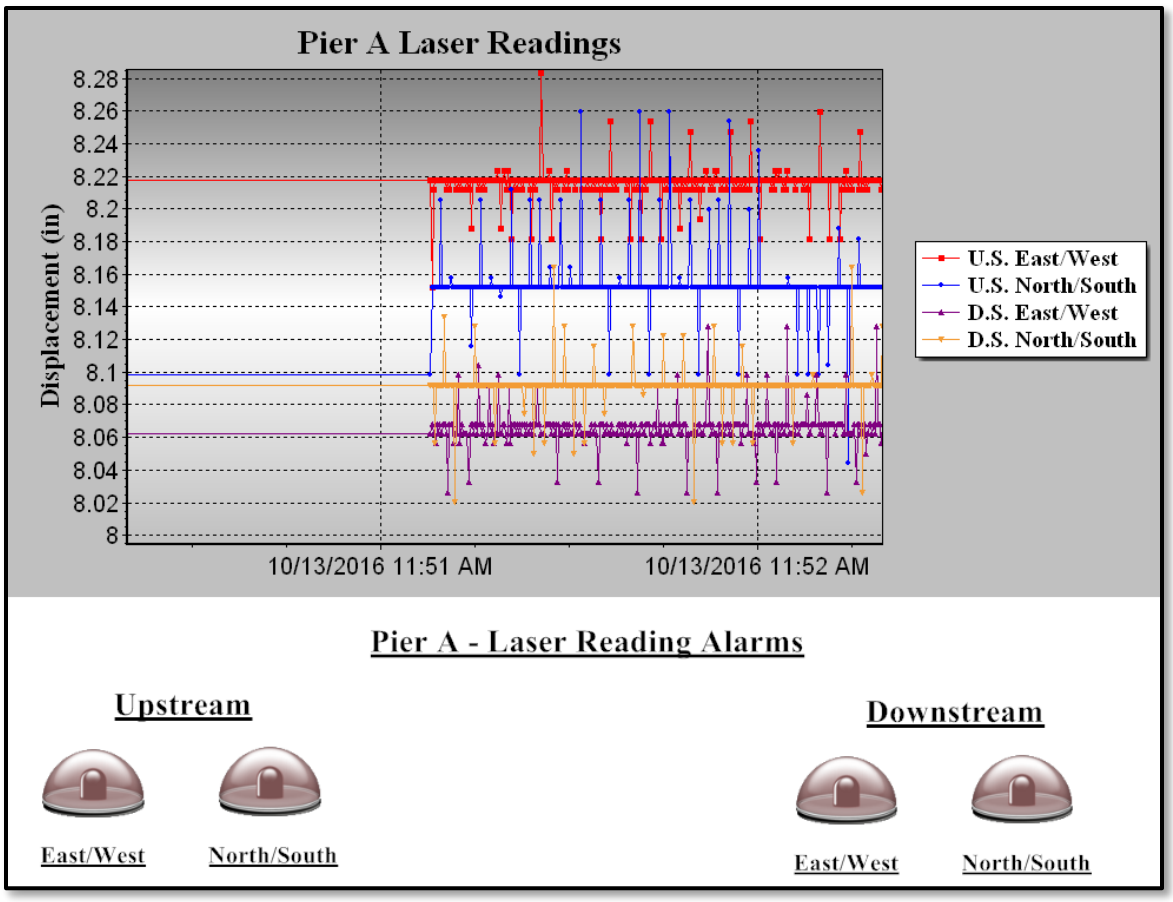

Figure 8.7 - Laser Sensor Interface

The selected threshold values for the real time monitoring display can be seen in **Error! Reference source not found.** below. The interface will trigger the alerting system and alert which gage and what threshold was exceeded, allowing the bridge owner to have the ability to be proactive to any gage malfunction or anomalies detected by the system.

Table 8.1 - Alarm Thresholds

Alarm Thresholds		
Pier A		
Displacement Thresholds		
Alarms	Minimum (in)	Maximum (in)
Main Bearings	-6.5	2.5
Approach Bearings	-6.5	2.5
Strain Thresholds		
Alarms	Minimum (MicroStrain)	Maximum (MicroStrain)
U.S. Vertical	-95	122
U.S. Diagonal	-153	49
U.S. Bottom	-87	73
D.S. Vertical	-191	161
D.S. Diagonal	-94	116
D.S. Bottom	-179	49
Laser Rading Thresholds		
Alarms	Minimum (ft)	Maximum (ft)
U.S. East/West	7	9
U.S. North/South	7.5	8.5
D.S. East/West	7	9
D.S. North/South	7.5	8.5
Pier C		
Displacement Thresholds		
Alarms	Minimum (in)	Maximum (in)
Main Bearings	-6.5	2.5
Strain Thresholds		
Alarms	Minimum (MicroStrain)	Maximum (MicroStrain)
U.S. Vertical	-138	67
U.S. Diagonal	-165	37
U.S. Bottom	-87	138
D.S. Vertical	-173	174
D.S. Diagonal	-179	79
D.S. Bottom	-164	186

8.2 Post Event Data Acquisition

In the event of an earthquake or any other significant event, TDOT and/or TTU will have the ability to access the displacement readings and strains readings captured by the

system. This will allow engineers to identify any movement the structure experienced during the earthquake and determine if the structural integrity of the bridge had been compromised due to the movement. In addition, the collected data will allow for proactive approaches to addressing any issues that may have occurred during the event. In this section, a general guide to analyzing the post-event data is provided to assist system users in identifying any anomalies and structural deficiencies that may have occurred on the bridge.

Upon the event of an earthquake, the first thing to do is check and compare the pre-event and post-event bearing position using the laser readings. If there was no change in the pre-event and post-event readings, this means one of two things: 1) there was no bearing movement due to the earthquake or 2) there was movement during the earthquake, and the bearings recovered to their pre-event location once the movement stopped. If there was a change between pre-event and post-event bearing location, laser sensors would need to be visually inspected to ensure they did not get displaced during the earthquake or detached from their sensor mounts. This will eliminate whether the change in bearing position is due to the sensors being displaced or the displacement of the structure. Next, post-event forces in the members must be checked and compared to the pre-event forces measured by the system. Event forces will not be captured due to the sampling rate designated for the VW gages. Pre and post-event force comparison will help identify any shifts the structure may have experienced from the earthquake. Member forces must be compared to their yield force to determine whether the change in bearing location was due to yielding members and possible deformation of members.

In addition to identifying bearings recovery and member forces, visual inspections must be performed to determine any damage done to the system. Visual inspection of strain gages and displacement gages needs to be done to ensure the gages did not get detached from members and that gages did not get bent or exceed movement capacity during the earthquake. Damaged or malfunctioning gages can also be confirmed by comparing any changes in post-event data with pre-event data. Once the gages and data have been reviewed and analyzed, cabling throughout the bridge and wire connections within the boxes must be visually inspected to verify the post-event gage readings are accurate. In addition, it would confirm if wire connections may have come apart due to the movement on the bridge. Cabling must be inspected and reattached to the existing hard conduit on the structure to prevent loose cabling from being hazardous to future personnel on the structure. Data quality will be jeopardized if instruments are not wired correctly. Furthermore, instruments in the boxes must be visually inspected as they may have been dislodged within the box during the movement on the structure.

CHAPTER 9

CONCLUSION AND FUTURE RESEARCH

A static-based SHM system was designed and installed along the Hernando DeSoto Bridge. This was due to its seismic vulnerability and its high importance to travelers crossing the Mississippi River. The objective of the system was to examine the performance and functionality of the friction pendulum bearings implemented in the seismic retrofit and provide a monitoring system to effectively capture the bearing movements and member forces before, during and after a seismic event. First, the system was designed through study of the bridge plans and inspection reports. Next the necessary instrumentation was ordered, and programs were developed for the system to provide high quality data. Once the system was checked, installation dates and necessities such as lane closures and the use of an Aspen A-62 snooper truck were coordinated with the University of Memphis CERI and TDOT. The system was then installed over a span of five days with one of the five days allocated for post install quality control checks. Data was collected and analyzed over a three-month period to study the bridge thermal movement / forces and determine bearing performance levels at Pier A and Pier C (primary findings provided below). In addition, a real-time monitoring display was developed for visualization of the data along with basic alerting criteria.

9.1 Pier A Investigation

To determine the Pier A bearing performance levels, thermal movements and member strains were analyzed. Bearing design characteristics such as the coefficient of friction in the bearings were compared to actual measured values collected from the system. The measured coefficient of friction was back calculated using the change in strain values collected during the early stick and late stick time frames established from the bearing displacement versus temperature relationship. This change in strain values during these time frames relates to the force build-up required to break friction in the bearings. The early and late stick time frames are time intervals where none to minimal movement occurs as temperature increases and decreases due to the friction in the bearings, respectively. This friction allows for member forces to build-up until the horizontal forces created by the temperature change exceed friction and release the build-up. More information on how the time frames were established and what data was selected to be used in the analysis can be reviewed in Sections 7.1.1 and 7.1.2.

By converting the strain to force values and summing the horizontal forces, a friction force was calculated for each bearing at each time frame. The coefficient of friction was then calculated using the estimated average dead load on the bearings from bridge plans provided by TDOT. With a coefficient of friction design value of 6%, the averages of the coefficient of friction for the Pier A upstream and downstream bearings was compared to the calculated values of 5% and 6%, respectively. The standard deviations

of the measured coefficient of friction values for the Pier A upstream and downstream bearings were also calculated to be 0.0063 and 0.0122, respectively. These results indicate the coefficient of friction still present after 15 years of service is nearly the same as initially constructed.

Theoretical and measured movements at Pier A were also compared. A linear regression analysis was performed to the collected data on the developed bearing displacement versus temperature graphs in order to determine the amount of movement per degree of temperature change. The reciprocals of the slope of the line of best fit for the Pier A upstream and downstream bearings were $0.077\frac{in}{°\mathrm{F}}$ and $0.079\frac{in}{°\mathrm{F}}$, respectively. With the assumption that the thermal neutral point was at Pier B and using the equation for linear thermal expansion, the expected theoretical movement was determined to be $0.0702\frac{in}{°\mathrm{F}}$. The larger measured values may imply the thermal neutral point is located closure to Pier C or the coefficient of thermal expansion used was slightly higher than estimated. In either case, based on the analysis and comparison of design to measured values, the Pier A friction pendulum bearings illustrated sufficient movement with temperature change.

9.2 Pier C Investigation

A similar investigation of the Pier C bearing functionality was performed using the monitoring system data. Through analyzing the data, it was determined that limited movement was occurring in the bearings and that further investigation was needed to

determine the cause of the limited movement. Using the late stick time frames established in the Pier A bearing performance investigation, average horizontal forces were calculated and compared to the average horizontal forces experienced at Pier A during the same time frame. It was calculated that 12% less force (or 38 kips) was measured between the bearings at Pier A and Pier C. The average horizontal force experienced in the bearings at Pier C was 88% of the designed force required to break friction within the bearings. If the sum of the horizontal forces in the bearings do not exceed friction, movement will not occur. This lack of force build-up with limited thermal movements implied the expected thermal movements may be occurring at other locations on the bridge. Theories for the lack of movement were developed and investigated.

Several theories were evaluated, but the likely reason for the limited bearing movement at Pier C was due to substructure movement. This theory was considered the most feasible due to the lack of strain build-up in the members. If the amount of force needed to break friction was greater than the amount of force needed to tilt the pier, the pier will tilt first before any movement will occur in the bearings. To further support this theory, the difference in the approach span lengths of Pier A and Pier C was thought to have an effect on the pier's ability to tilt. The span length of the approach of Pier C is substantially smaller than the approach span length at Pier A. The longer the span length, the larger the thermal movement and the larger potential force produced by temperature change. The approach span of Pier A also frames onto friction pendulum bearings which have a greater coefficient of friction than the lead-rubber bearings implemented on the approach span of Pier C. The combination of the friction in the lead-rubber bearings and

the thermal expansion of the shorter approach span at Pier C may not produce enough force to counteract the thermal forces produced by the arches causing the substructure to tilt. This theory cannot be validated without upgrades to the existing system, however, it would explain the lack of strain build-up in the members framing into the friction pendulum bearings at Pier C. Overall, the Pier C bearing performance could not be determined through this investigation, but theories for the lack of thermal movement were developed to provide means for future research on the Hernando DeSoto Bridge.

9.3 Real-Time Monitoring System

A real-time monitoring display was developed with basic alerting capabilities and threshold criteria in order to allow users to monitor the structure in real time. The interface included bearing displacement time history graphs and strain time history graphs to show how the measured displacements and strains fluctuate throughout the day. These displays include alarms with specified thresholds to alert users of data anomalies that may occur. Displacement versus temperature relationships were also developed to display the cyclic movement of the bearings with respect to temperature and monitor the natural pattern to detect structural anomalies that may disrupt the movement. A laser reading interface was developed with alarms to alert users of large bearing displacements, capture the potential larger bearing movements and display the bearing movements before, during and after a seismic event. With the created real-time interface, engineers will have the ability to

monitor the structure in real time and provide proactive approaches to addressing future data anomalies.

9.4 Future Research and System Improvements

The development of the SHM system implemented on the Hernando DeSoto Bridge has provided TDOT with information on the performance and functionality of the friction pendulum bearings at Pier A and Pier C, but it has also raised questions about the thermal behavior of the structure. Further research can be done by investigating the proposed theories presented in the section 7.2.2 for the limited movement measured at Pier C. In doing so, upgrades to the system, such as the implementation of a tilt meter and/or a non-contact displacement gage, can be done to effectively capture the Pier C substructure's global movements and validate or disprove the presented theories.

Other additions to the system would be to implement a set up containing strain gages and displacement gages to study thermal behavior at Pier B. Having information on the thermal behavior at Pier B would give insight to the performance of the friction pendulum bearings on that pier and enhance the understanding of the thermal movement throughout the main section of the bridge. Suggestions for this addition would be to implement displacement gages at the bearings and instrument the arch members framing into the bearings at Pier B with strain gages to capture the strain experience in the members as the bridge heats up and cools down.

Along with the addition of the set up at Pier B, additional dataloggers can be implemented at each pier on the main section in order to prevent any measurements from being lost to frequency inferences from the city of Memphis. A datalogger at each pier would allow the wirelessly transmitted measurements to be saved on the datalogger and resent at the end next measurement reading when the wirelessly transmitted readings are interfered. Strain gages can be also attached to the instrumented members on all the piers of the main section to aid in deciphering between axial strains and out-of-plane bending. This would provide more pertinent information on the amount of axial strain and out-of-plane bending occurring on the structure.

Furthermore, code can be developed to automate the SHM system. The automated system would have the ability to send email alerts of data anomalies by exceeding specific thresholds. With this upgrade, emails would be sent to the bridge owner containing information on the anomaly and/or what threshold was exceeded enabling a more proactive approach to monitoring and preserving the Hernando DeSoto Bridge long term.

REFERENCES

1. 2015 National Bridge Inventory ASCII. American Road and Transportation Builders Association (January 2016), http://www.artba.org/economics/2016-u-s-deficient-bridges/ . Accessed 8 Sept. 2016.

2. *Interstate 40 Hernando DeSoto Bridge*. Tennessee Department of Transportation Database, https://www.tn.gov/tdot/topic/i-40-hernando-desoto-bridge . Accessed 14 Sept. 2016.

3. Shahram, P., Withers, M., and Steiner, G. "Seismic Instrumentation at the I-40 Hernando Desoto Bridge in Memphis, Tennessee." *Structural Congress* (2006).

4. Catbas, F. N. "Structural health monitoring: applications and data analysis." *Structural Health Monitoring of Civil Infrastructure Systems* (2009): 1.

5. Kim, S., D. Culler, and J. Demmel. "Structural Health Monitoring of the Golden Gate Bridge Using Wireless Sensor Networks".

6. De Roeck, G. "The state-of-the-art of damage detection by vibration monitoring: the SIMCES experience." *Journal of Structural Control*, 2003. 10.2: 127-134.

7. Peeters, B. and G. De Roeck. "One-year monitoring of the Z24-Bridge: environmental effects versus damage events." *Earthquake Engineering & Structural Dynamics*, 2001. 30(2): p. 149-171.

8. Omenzetter, P. and Brownjohn, J.M.W. "A Seasonal ARIMAX Time Series Model for Strain-Temperature Relationship in a Instrumented Bridge", in *Structural Health Monitoring*, F.K. Chang, Editor, 2005. p. 299-306.

9. Howell, D. and H. Shenton. "System for In-Service Strain Monitoring of Ordinary Bridges." *Journal of Bridge Engineering*, 2006. 11(6): p. 673-680.

10. Enckell, M., Glisic, B., Myrvoll, F., and Bergstrand, B. (2011). "Evaluation of a large-scale bridge strain, temperature and crack monitoring with distributed fiber optic sensors." *Journal of Civil Structural Health Monitoring, 1*(1-2), 37-46.

11. Leung, C. K., Wan, K. T., Inaudi, D., Bao, X., Habel, W., Zhou, Z., Ou, J., Ghandehari, M., Wu, H.C., and Imai, M. (2015). "Review: optical fiber sensors for civil engineering applications." *Materials and Structures*, *48*(4), 871-906.

12. Serker, N.H.M. Kamrujjaman, and Wu, Z.S. "Structural health monitoring using static and dynamic strain data from long-gage distributed FBG sensor." IABSE-JSCE Joint Conference on Advances in Bridge Engineering-II 2010 (2010).

13. Yarnold, M. T. and F.L. Moon. (2015). Temperature-based structural health monitoring baseline for long-span bridges. *Engineering Structures*, *86*, 157-167.

14. Gilstad, D., "Bridge Bearing and Stability". *Journal of Structural Engineering*, 1990. 116(5): p. 1269-1277.

15. Yarnold, M.T. and N. C. Dubbs "Bearing Assessment using Periodic Temperature-Based Measurements" (2015).

16. Cachot, E., T. Vayssade, M. Virlogeux, H. Lancon, Z. Hajar and Claude Servant. "The Millau Viaduct: Ten Years of Structural Monitoring". *Structural Engineering International* (2015).

17. Chan, T. H., Yu, L., Tam, H. Y., Ni, Y. Q., Liu, S. Y., Chung, W. H., and Cheng, L. K. (2006). "Fiber Bragg grating sensors for structural health monitoring of Tsing Ma Bridge: Background and experimental observation." *Engineering structures*, 28(5), 648-659.

18. Herman, R., et. al., "Performance Of Steel Bridges Under Thermally Induced Loads", in *World Steel Bridge Symposium*. 2007.

19. Wang, G., et. al., "Detection and Location of the Degraded Bearings Based on Monitoring the Longitudinal Expansion Performance of the Main Girder of the Dashengguan Yangtze Bridge", in *Journal of Performance of Constructed Facilities*, 30(5), 2016.

APPENDIX: SYSTEM PROGRAM

```
'De Soto Main Program.CR1
'Pipeline Mode
'Hernando De Soto SHM System
'Date Revised:8/27/16
'Program Author:Justin Alexander

' Constants

    Const  SR           = 5      'Scan Rate in Minutes
    Const  SR_L         = 100    'Scan Rate of Lasers in milliseconds
    Const  Strain_BFreq = 450    'Beginning Frequency of Strain Gages
    Const  Strain_EFreq = 1250   'End Frequency of Strain Gages
    Const  Displ_BFreq  = 1200   'Beginning Frequency of Displacement Gages
    Const  Displ_EFreq  = 2800   'End Frequency of Displacement Gages
    Const  VW_Total     = 30     'Total Number of VW Gauges
    Const  VW_Scan      = 2.5    'Time Needed in Seconds to Scan 1 VW Gauge
    Const  MuxChan1     = 1      'Starting Mux Channel of Strain Gages in both Box A & C
    Const  MuxChan2     = 13     'Starting Mux Channel of Displ. Gages in both Box A & C

  'Box A

          Const  Reps_StrainAVW200       = 12    'Number of Strain gauges on AVW200
          Const  Reps_DisplacementAVW200 = 4     'Number of Displacement gauges on AVW200
          Const  Reps_Laser              = 4     'Number of Lasers in Box A
          Const  PakBusA                 = 200   'PakBus Address of AVW200 in Box A


  'Box C

          Const  Reps_StrainAVW206       = 12    'Number of Strain gauges on AVW206
    Const  Reps_DisplacementAVW206 = 2     'Number of Displacement gauges on AVW206
    Const  PakBusC                 = 201   'PakBus Adrees of AVW206 in Box C

 'Laser Variables

    Const  RB    = 2          '4 mAmp reading threshold in feet
    Const  RE    = 30         '20 mAmp reading threshold in feet
    Const  L_CF  = 0.01       'Conversion from MilliVolts to MilliAmps on Laser readings


 'Temperature Coversions Constants for Strain and Displacement - Resistance to Degrees C

     Const A = .0014051
     Const B = .0002369
     Const C = .0000001019

  'Averaged Gauge Factor and Conversion Factor for Displacement Gauges

       Const GF = .001818     'inches per digit (Averaged value from all dispalcement gauges
```

Figure A. 1 - Page One of System Code

```
'Public Constants


           Public PTemp, batt_voltA, BattResults, batt_voltC

'Lasers

  Public AR1000_Feet(Reps_Laser), AR1000_mAmps(Reps_Laser)

'Strain Gauges

  Public Straindirect(Reps_StrainAVW200), Strainwireless(Reps_StrainAVW206)
  Public Sresultsdirect, Sresultswireless, Svaluesdirect(Reps_StrainAVW200,6),
         Svalueswireless(Reps_StrainAVW206,6)

  Public SDigitsdirect(Reps_StrainAVW200)
  Public SDigitswireless(Reps_StrainAVW206)

  Public StrainTempDirect(Reps_StrainAVW200,1)
  Public StrainTempWireless(Reps_StrainAVW206,1)

'Displacement Gauges

  Public Displacementdirect(Reps_DisplacementAVW200), Displacementwireless(Reps_DisplacementAVW206)
  Public Dresultsdirect, Dresultswireless, Dvaluesdirect(Reps_DisplacementAVW200,6),
         Dvalueswireless(Reps_DisplacementAVW206,6)

  Public DDigitsdirect(Reps_DisplacementAVW200)
  Public DDigitswireless(Reps_DisplacementAVW206)

  Public DisplacementTempDirect(Reps_DisplacementAVW200,1)
  Public DisplacementTempWireless(Reps_DisplacementAVW206,1)



'Dimension

  Dim I, J, K


'Data Table Declarations

  DataTable (VW_Results,1,-1)
  DataInterval(0,SR,Min,SR)
  CardOut(0,-1)
```

Figure A. 2 - Page Two of System Code

```
'Data Table Declarations

  DataTable (VW_Results,1,-1)
  DataInterval(0,SR,Min,SR)
  CardOut(0,-1)

'Box A - Strain Gauges and Displacement Gauges sampled in Data Table

  Sample (Reps_StrainAVW200,Straindirect(),IEEE4)
  'Sample (Reps_StrainAVW200*6,Svaluesdirect(),IEEE4)
       'Raw values from strain gauges,commented out to have
       more memory for lasers

  Sample (Reps_DisplacementAVW200,Displacementdirect(),IEEE4)
  'Sample (Reps_DisplacementAVW200*6,Dvaluesdirect(),IEEE4)
       'Raw values from displ. gauges,commented out to have
       more memory for lasers

  Sample (Reps_StrainAVW200,StrainTempDirect(),IEEE4)
       'Sampling of Strain Temperature

  Sample (Reps_DisplacementAVW200, DisplacementTempDirect(),IEEE4)
       'Sampling of Displacement Temperature


'Box C - Strain Gauges and Displacement Gauges sampled in Data Table

  Sample (Reps_StrainAVW206,Strainwireless(),IEEE4)
  ' Sample (Reps_StrainAVW206*6,Svalueswireless(),IEEE4)
  Sample (Reps_DisplacementAVW206,Displacementwireless(),IEEE4)
  'Sample (Reps_DisplacementAVW206*6,Dvalueswireless(),IEEE4)

  Sample (Reps_StrainAVW206, StrainTempWireless(),IEEE4)
       'Sampling of Strain Temperature

  Sample (Reps_DisplacementAVW206,DisplacementTempWireless(),IEEE4)
       |'Sampling of Displacement Temperature

'Temperature and Battery

  Sample (1,PTemp,FP2)
  Sample (1,batt_voltA,FP2)

EndTable

'Data Table - Battery Voltage for Box C

  DataTable (BattResults,1,-1)
  DataInterval (0,SR,Min,SR)
  Sample (1,batt_voltC,IEEE4)
EndTable
```

Figure A. 3 - Page Three of System Code

```
'Data Table - Laser Readings

  DataTable (Laser_Readings,1,-1)
  DataInterval (0,SR_L,msec,1000)
  CardOut(0,-1)
  Sample (Reps_Laser,AR1000_Feet(),IEEE4)
EndTable


' Main Program

  BeginProg

   SerialOpen(Com1,38400,0,0,0)
        'Opens serial port for direct connection to AVW200

    Scan(SR,Min,0,0)
        'Scan of all VW gauges & Lasers

     PanelTemp (PTemp,250)
     Battery (batt_voltA)
     GetVariables (BattResults,ComSDC7,0,PakBusC,0,0,"Status",
                   "BattVoltage",batt_voltC,1)
        'Retrieves Battery Voltage from Box C

'Box A VW Scanning

  AVW200(Sresultsdirect,Com1,0,PakBusA,Svaluesdirect(),1,MuxChan1,
         Reps_StrainAVW200,Strain_BFreq,Strain_EFreq,1,_60Hz,1,0)
        'Scanning Strain in AVW200

  AVW200(Dresultsdirect,Com1,0,PakBusA,Dvaluesdirect(),1,MuxChan2,
         Reps_DisplacementAVW200,Displ_BFreq, Displ_EFreq, 1,_60Hz,1,0)
        'Scanning Displacement in AVW200

'Box C VW Scanning

  AVW200(Sresultswireless,ComSDC7,0,PakBusC,Svalueswireless(),1,MuxChan1,
         Reps_StrainAVW206,Strain_BFreq,Strain_EFreq,1,_60Hz,1,0)
        'Scanning Strain in AVW206

  AVW200(Dresultswireless,ComSDC7,0,PakBusC,Dvalueswireless(),1,MuxChan2,
         Reps_DisplacementAVW206,Displ_BFreq, Displ_EFreq, 1,_60Hz,1,0)
        'Scanning Displacement in AVW206
```

Figure A. 4 - Page Four of System Code

```
'Laser Subscan to get Laser Readings at 10 Hz

 SubScan(SR_L,msec,((SR*60)*1000/SR_L)

  VoltDiff(AR1000_mAmps(),Reps_Laser,AutoRange,1,True,0,250,L_CF,0)

   'Converting Laser milliamp readings into feet using interpolation

    For K = 1 To Reps_Laser
       'Interpolating milliamp laser readings into feet

    AR1000_Feet(K) = ((AR1000_mAmps(K)-4)/(20-4))*(RE-RB)+RB
    Next K

    CallTable (Laser_Readings)

 NextSubScan

'Conversions

'Box A (direct)

 For I=1 To Reps_StrainAVW200

  SDigitsdirect(I) = (Svaluesdirect(I,1))^2/1000
        'Frequency to Digits

  Straindirect(I) = SDigitsdirect(I)*4.062*.96
       'Digits to Strain (microstrain)

  StrainTempDirect(I) = (1/(A+B*(LN(Svaluesdirect(I,6)))+
                         C*(LN(Svaluesdirect(I,6)))^3)-273.2)*1.8+32
        'Resistance to Farenheit

 Next I

 For I=1 To Reps_DisplacementAVW200

  DDigitsdirect(I) = (Dvaluesdirect(I,1))^2/1000
        'Frequency to digits

  Displacementdirect(I) = GF*DDigitsdirect(I)
        'Digits to Inches

  DisplacementTempDirect(I) = (1/(A+B*(LN(Dvaluesdirect(I,6)))+
                              C*(LN(Dvaluesdirect(I,6)))^3)-273.2)*1.8+32
        'Resistance to Farenheit

 Next I

  PTemp = PTemp*1.8 + 32      'Panel Temp converted to Farenheit
```

Figure A. 5 - Page Five of System Code

```
'Box C (wireless)

  For J=1 To Reps_StrainAVW206
   SDigitswireless(J) = (Svalueswireless(J,1))^2/1000
          'Frequency to Digits on Strain Gauges

   Strainwireless(J) = SDigitswireless(J)*4.062*.96
          'Digits to Inches on Strain Gauges

   StrainTempWireless(J) = (1/(A+B*(LN(Svalueswireless(J,6)))+
                            C*(LN(Svalueswireless(J,6)))^3)-273.2)*1.8+32
  Next J

  For J=1 To Reps_DisplacementAVW206
   DDigitswireless(J) = (Dvalueswireless(J,1))^2/1000
          'Frequency to Digits on Displacement Gauges

   Displacementwireless(J) = GF*DDigitswireless(J)
          'Digits to Inches on Displacement Gauges

   DisplacementTempWireless(J) = (1/(A+B*(LN(Dvalueswireless(J,6)))+
                                  C*(LN(Dvalueswireless(J,6)))^3)-273.2)*1.8+32
          'Resistance to Farenheit

  Next J



    CallTable (VW_Results)
    CallTable (BattResults)


                NextScan


         EndProg
```

Figure A. 6 - Page Six of System Code

VITA

Justin Ryan Bravo Alexander was born on February 18, 1992 on the island of Saipan, an island part of the Northern Marianas Islands in the South Pacific. He lived in Saipan until the summer of 2006 where he would then move to Knoxville, Tennessee to attend high school at The Webb School of Knoxville. He graduated high school in May 2010. Upon graduation, he began attending Tennessee Technological University in the fall of 2010 to pursue a degree in Civil Engineering while playing Division I baseball. He passed the Fundamentals of Engineering Exam in January of 2015. He would graduate cum laude with a Bachelor of Science in Civil and Environmental Engineering with a focus in Structural Engineering in May 2015. The following semester, he began to pursue his Masters of Science Degree in Civil Engineering with a concentration in Structural Engineering and graduated in the spring of 2017.